SCIENCE CHINA
Earth Sciences

•PROGRESS•

September 2021 Vol.64 No.9: 1504–1523
https://doi.org/10.1007/s11430-020-9789-2

Conditions and processes leading to large-scale gold deposition in the Jiaodong province, eastern China

Hongrui FAN[1,2,3*], Tingguang LAN[3,4], Xinghui LI[1,3], M. SANTOSH[5], Kuifeng YANG[1,2,3], Fangfang HU[1,2,3], Kai FENG[1,2,6], Huanlong HU[1,2,4], Hongwei PENG[1,2,7] & Yongwen ZHANG[1,2]

[1] *Key Laboratory of Mineral Resources, Institute of Geology and Geophysics, Chinese Academy of Sciences, Beijing 100029, China;*
[2] *College of Earth and Planetary Sciences, University of Chinese Academy of Sciences, Beijing 100049, China;*
[3] *Innovation Academy for Earth Science, Chinese Academy of Sciences, Beijing 100029, China;*
[4] *State Key Laboratory of Ore Deposit Geochemistry, Institute of Geochemistry, Chinese Academy of Sciences, Guiyang 550081, China;*
[5] *State Key Laboratory of Geological Processes and Mineral Resources, China University of Geosciences Beijing, Beijing 100083, China;*
[6] *State Key Laboratory of Mineral Processing, BGRIMM Technology Group, Beijing 102628, China;*
[7] *School of Geosciences and Info-physics, Central South University, Changsha 410012, China*

Received November 25, 2020; revised April 29, 2021; accepted May 11, 2021; published online July 15, 2021

Abstract The gold deposits in the Jiaodong Peninsula constitute the largest gold mineralized province in China. The mineralization shows common characteristics in their tectonic setting, ore-forming fluid and metallogenic system. Sulfidation and fluid immiscibility are two important mechanisms controlling gold precipitation, both of which consume sulfur in the ore-forming fluids. The escape of H_2S from the main ore-forming fluids and the decrease of total sulfur concentration not only lead to the efficient precipitation of gold, but also result in the crystallization of reducing minerals such as pyrrhotite and oxidizing minerals such as magnetite. Quartz solubility shows strong dependence on temperature, pressure, and CO_2 content. The dependence of quartz solubility on pressure is weak at low temperatures, and progressively stronger at higher temperatures. Similarly, the temperature dependence of quartz solubility is relatively low at low pressures, but becomes gradually stronger at high pressures. The results of solubility modeling can constrain the dissolution and reprecipitation behavior of quartz in the ore-forming veins and the formation mechanism of different types of quartz veins. The multi-stage mineralization fluid activity resulted in the complex dissolution structure of quartz in the Jiaodong gold veins. Pyrite in the main metallogenic period in the Jiaodong gold deposits shows complex microstructure characteristics at single crystal scale. The trace elements (mainly the coupling of As- and Au-rich belt) and sulfur isotope composition also display a certain regularity. The As-rich fluids might have formed by the initial pulse of ore-forming fluids through As-rich metasedimentary strata, while the As-Au oscillation zone at the margin of pyrite grains is related to the pressure fluctuation caused by fault activity and the local phase separation of fluids. There is a temporal and spatial evolution of gold fineness in the Jiaodong gold deposits. Water/rock reaction (sulfidation) was the main ore-forming mechanism of early gold mineralization, forming relatively high fineness gold, while significant pressure drop in the shallow part accompanied by fluid phase separation promoted the late gold mineralization, forming low fineness gold. Under cratonic destruction setting, dehydration of the amphibolite and granulite facies metamorphic lower-crust resulted in the formation of Au-CO_2-rich ore-forming fluids, which rose along the deep fault and secondary structure, and formed the large-scale fault-controlled gold deposits in Jiaodong.

Keywords Mineral precipitation, Mineral assemblage, Gold fineness, Ore-forming condition and processes, Gold deposit, Jiaodong

Citation: Fan H, Lan T, Li X, Santosh M, Yang K, Hu F, Feng K, Hu H, Peng H, Zhang Y. 2021. Conditions and processes leading to large-scale gold deposition in the Jiaodong province, eastern China. Science China Earth Sciences, 64(9): 1504–1523, https://doi.org/10.1007/s11430-020-9789-2

* Corresponding author (email: fanhr@mail.iggcas.ac.cn)

© Science China Press and Springer-Verlag GmbH Germany, part of Springer Nature 2021

1. Introduction

Mineralization refers to the geological process that involves the transport of useful components (elements or compounds) from the source, migration, and accumulation to form ore deposits in the shallow crust. Hence, source, migration and accumulation of ore elements are the three basic issues in the ore deposit researches. Constraints on mineralization mainly focuses on the conditions and processes that cause ore deposition and controls the distribution regularities of ore bodies. As the final stage of the prolonged mineralization history, detailed study of metal accumulation can be used to reveal the "source" and trace the "migration" of metal elements. Formation of large and super-large hydrothermal deposits usually reflects continuous or multistage fluid supply and circulation (Moncada et al., 2019). During this process, elements, isotopes, minerals, and fluid compositions inevitably change through time and space. Understanding of those changes and their controls can provide significant constraints on the sources of ore-forming materials, the mechanism of element transport and mineral precipitation, and the genesis of hydrothermal deposits.

Jiaodong is the most gold concentrated province in China, where a strong correspondence exists between gold mineralization and the peak of destruction of the North China Craton (Zhu et al., 2015). This paper starts with the thermodynamic prediction and simulation of the evolution of minerals assemblage from typical gold deposits in the northeastern Jiaodong. Based on this method, we discuss the thermodynamic mechanism of gold precipitation that was caused by total sulfur concentration and the control of CO_2 fluid system immiscibility and quartz dissolution-precipitation on gold mineralization. Subsequently, through analyzing the micro-domain element and isotopic geochemical characteristics and mineral micro-growth history of pyrite from different mineralization stages, we describe the time evolution of trace elements and isotopes in each mineralization stage, and discuss the precipitation mechanism of gold and spatiotemporal evolution of gold fineness. Finally, we propose a novel conceptual model for the genesis of the Jiaodong gold deposits, which is similar to the orogenic gold deposit resulting from high-grade metamorphism.

2. Geologic setting of metallogeny and geologic features of gold deposits

2.1 Regional geologic background

The Jiaodong Peninsula is located on the southeastern margin of the North China Craton (NCC). The region is bound by the Tan-Lu fault in the west and adjacent to the Luxi block. The Jiaodong region is separated by the Wulian-Yantai fault into two structural units, the Jiaobei terrain and the Sulu ultra-high pressure (UHP) metamorphic belt (Figure 1). The rocks in this region mainly include Precambrian basement rocks, which are composed of the Late Archean Jiaodong Group (TTG gneiss, amphibolite and granulite), Paleoproterozoic Jingshan Group and Fenzishan Group (high greenschist facies-high amphibolite facies metamorphic rocks) and the Neoproterozoic Penglai Group (low-greenschist facies metamorphic rocks), Triassic ultrahigh-pressure metamorphic rocks and Late Mesozoic magmatic rocks which are composed of the Late Jurassic Linglong and Luanjiahe monzonitic granites (160–157 Ma; Miao et al., 1997), Early Cretaceous Guojialing granodiorite (130–126 Ma; Yang et al., 2012), Early Cretaceous Aishan granite (118–115 Ma; Li et al., 2018a) and mafic-felsic dykes (132–86 Ma; Cai et al., 2013).

Since the Mesozoic, due to the subduction of the Yangtze plate and the Pacific plate and the change in the direction-angle of the subduction, the Jiaodong Peninsula has witnessed a complex history of tectonic evolution, with numerous transformations in the stress field (Sun et al., 2007; Deng et al., 2015). The Yangtze plate and the North China plate collided during the Triassic inducing a compression tectonic setting (Zheng et al., 2013). The compressional setting transformed to extension because of the delamination after collision and the Pacific plate subduction at 160–140 Ma. Afterwards, the Jiaodong region was in an extensional background as a whole, but a brief transitional compression regime occurred due to the direction-angle change of the subduction of the Pacific plate at 125–122 Ma. Finally, the tectonic setting became an extensional through the subduction-rollback of the Pacific plate at approximately 110 Ma. The Craton destruction and related gold mineralization occurred at 130–120 Ma (Zhu et al., 2015; Zheng et al., 2018; Wu et al., 2019b; Zheng et al., 2019).

2.2 Geological features of gold deposits

The Jiaodong province hosts several gold deposits with substantial gold reserves. In the past ten years, the Exploration Breakthrough Strategy Action has discovered 4600 tons of gold resources in the deep part of Jiaodong, which makes Jiaodong the third largest gold concentrated area in the world (Song et al., 2019). The Jiaodong gold province can be divided into three gold mineralizing belts, from west to east, the Zhaoyuan-Laizhou, Penglai-Qixia and Muping-Rushan gold belts. The Zhaoyuan-Laizhou belt is the most important, in which there are the most gold reserves and many large and super-large gold deposits, such as Sanshandao, Haiyu, Xiling, Xincheng, Tengjia, Jiaojia, Shaling, Sizhuang, Linglong, Yin'gezhuang and Shuiwangzhuang gold deposits (Figure 1).

Gold deposits in the Jiaodong province can be divided into two types, sulfide-bearing quartz vein type and fracture-al-

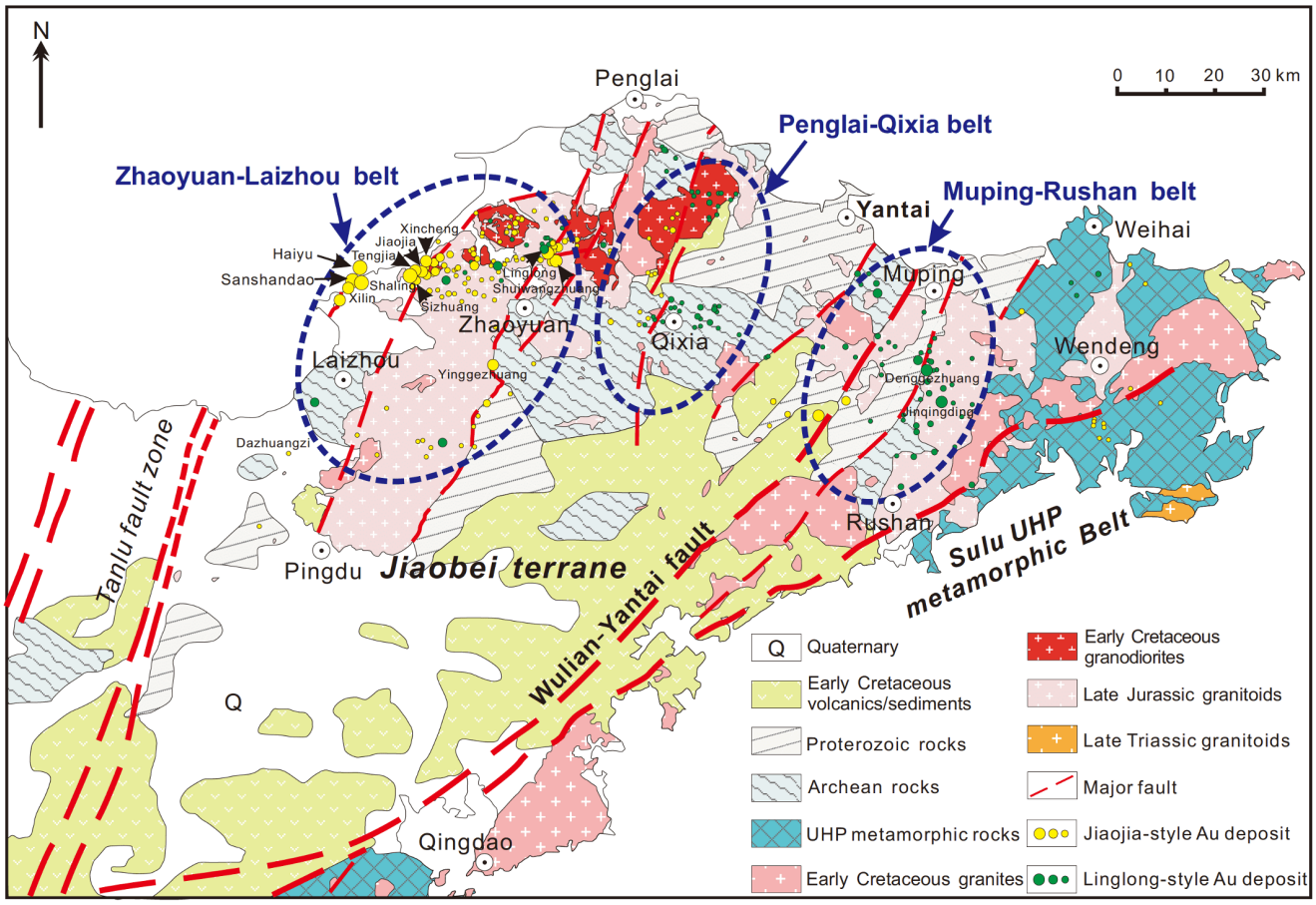

Figure 1 Simplified geological map of the Jiaodong Peninsula showing the major tectonic units and location of the major gold deposits (after Fan et al., 2003). The size of symbols for gold deposits indicates the relative volume of gold resources: The largest symbol corresponds to Au>50 t, and the smallest symbol means Au<10 t.

tered rock type. The minor type of gold mineralization belonging to ductile-brittle shear zone type at the margin of the basin can be classified as fracture-altered rock type. The sulfide-bearing quartz vein type gold deposits, also known as "Linglong-style" gold deposits, are characterized by multistage gold-bearing sulfide veins superimposed on favorable structural positions of large-scale quartz veins. Ore bodies are generally filled in the secondary structures of regional fractures, which can reach several kilometers in strike, range from tens of centimeters to more than ten meters in width, and extend obliquely from hundreds of meters to more than 1 km. The fracture-altered rock type gold deposits, also known as "Jiaojia-style" gold deposits, are mainly developed in the lithological contact interface between basement metamorphic rocks and Mesozoic granites, and within the NE-NNE-trending fault zone where the Mesozoic granites are partially intersected. The distribution of "Jiaojia-style" gold deposits is strictly controlled by the regional scale and gently inclined main fault zone, fragmentation zone and alteration zone. The ore bodies are often hosted in the footwall of the fault zone by disseminated and stockwork-style, and the fault zone is subjected to extensive fragmentation deformation and hydrothermal alteration.

Research on the alteration zone of typical gold deposit (Li et al., 2013) shows that hydrothermal fluids ascended through faults and caused fluid-rock reactions of varying degrees and scales in the wallrocks on both sides. Symmetrical alteration zoning often occurs in the quartz veins-type gold deposit. However, in the fracture-altered rock type gold deposit, the wallrock alteration in the footwall of fracture is generally more intense. Based on the multistage activity of the fault, hydrothermal pulsation and alteration superimposition, the following sequence and features of wallrock alteration are identified in the Jiaodong gold deposits. (1) Early hydrothermal activity produced extensive potassic alteration and silicification on both sides of the fault. (2) Large-scale sericification was superimposed on the potassium-silicification zone. (3) Subsequently, silicification of varying scale occurred, which was mainly superimposed on the sericification zone. (4) The gently dipping main fault zone was reactivated, forming a dense gray-white or black fault gouge near the fracture surface. This fault gouge is impermeable for later fluids to move upward into the hanging wall, causing the wallrock alteration and mineralization

in the hanging wall to be weak. (5) Fluid-rock interaction between the ore-forming fluids and the altered rocks in the footwall resulted in strong pyrite-sericite-quartz alteration with gold mineralization accompanied by the precipitation of polymetallic sulfides. (6) The last stage carbonation and quartz-carbonate veins, interspersed in the early alteration zones, marked the waning of gold-related hydrothermal activity. Thus, from the near orebody (main fracture surface) to the wallrock, the altered rocks are pyrite-sericite-quartz, sericite-quartz, sericitized cataclastic rock, potassic granite or metamorphic rock.

The gold mineralization in Jiaodong has the characteristic of multistage superimposed enrichment, and the multistage tectonic-metallogenic hydrothermal activities control gold mineralization. The mineralization can be divided into four stages as follows: (I) barren quartz stage, (II) gold-pyrite-quartz stage, (III) gold-polymetallic sulfide-quartz stage and (IV) quartz-calcite (-siderite) stage. The stage II and III are the main gold mineralization episode (Fan et al., 2016). The mineral assemblage of the two types of gold deposits is similar, mainly including pyrite, chalcopyrite, sphalerite, galena, pyrrhotite, arsenopyrite, magnetite and native gold, and electrum. Gangue minerals are mainly quartz, plagioclase, a small amount of potassium feldspar, white mica (sericite), ankerite, calcite, siderite and barite.

In the previous works on the timing of mineralization of the Jiaodong gold deposits, many scholars obtained data using sericite or muscovite Ar-Ar dating, K-feldspar K-Ar dating, and pyrite Rb-Sr dating, etc., and the results fall in the range of 130–100 Ma. (e.g., Yang and Zhou, 2001; Li et al., 2006). In the last decade, following the development of new technologies and methods, high-precision *in-situ* dating have been achieved. SHRIMP/LA-ICP-MS U-Pb dating of hydrothermal zircons and monazites in ore-bearing veins has been carried out to obtain accurate ages, with the gold mineralization time constrained as 120±5 Ma (Hu et al., 2013; Ma et al., 2017; Yang et al., 2018; Deng et al., 2020; Zhang L et al., 2020). The mineralization ages of Jiaodong gold deposits with different mineralization types or from different districts in the three gold belts are remarkably consistent, indicating that the gold mineralization occurred during a short period of time under the same metallogenic structure background and fluid mineralization system. Different tectonic stress may lead to the development of different mineralization styles. The main fault structure in the deposit district commonly controls the fracture-altered rock type gold deposit, and the small-scale secondary structure associated or derived from the main fault often controls the sulfide-bearing quartz vein type gold deposit. In the section dominated by compression-torsional faults, the pyrite sericite belt is developed, which mainly controls the altered rock-style gold deposits; in the section where torsional faults dominate, the mixed type of the sulfide-bearing quartz vein and the fracture-altered rock type occur; in the section dominated by tensional or transtensional fractures, or where extension fractures and fissures have developed, the major type is sulfide-bearing quartz vein gold deposits.

3. Thermodynamic environment of mineral paragenesis and gold deposition

The mineral paragenesis is consistent among Jiaodong gold deposits and only some of the deposits lack of arsenic-rich pyrite or arsenopyrite (Mills et al., 2015a; Li et al., 2018b; Hu et al., 2020b; Zhang Y W et al., 2020). Fluid inclusion microthermometry results indicate that the mineralization evolved along decreasing temperature trend, with no overprint of later higher temperature ore-forming fluid, and the H-O isotopic compositions do not suggest any different sources of fluids added into ore-forming system (Fan et al., 2003; Wang et al., 2015; Wen et al., 2015, 2016; Ma et al., 2018). These studies indicate that the ore-forming fluids were uniform among all Jiaodong gold deposits. However, the mineral assemblages are seemingly inconsistent with above results. On the one hand, several studies proposed that a stage of oxidizing ore-forming fluid pulsed into ore-forming system based on the occurrence of magnetite and barite in the mineralized veins (Mills et al., 2015b; Yang et al., 2018). On the other hand, stage III with precipitation of polymetallic sulfides contains pyrrhotite-(magnetite) assemblage (e.g., the Sanshandao, Jiaojia, Sizhuang, Xingcheng, Linglong, Hushan, Zhuangzi gold deposits), in which pyrrhotite indicates a reduced condition for ore-forming fluids (Wen et al., 2015, 2016; Yang et al., 2016; Hu et al., 2020a). The magnetite, pyrrhotite and barite, although of minor occurrence in veins, could be sensitive indicators for redox conditions of fluid. Therefore, the precipitation or coexistence of these minerals indicate that the ore-forming fluids experienced complex physicochemical evolutions in the Jiaodong gold deposits, and the possibility of multistage fluid pulses with different sources or single-sourced fluid evolution need more investigation. If the single-source ore-forming fluid evolution is the main case, it is difficult to reconcile with the thermodynamic connection among ore-forming fluid evolution, mineral assemblage evolution and gold deposition. Given these facts, it is necessary to carry out thermodynamic calculations to constrain the connection among them.

3.1 Thermodynamic prediction for mineral assemblage evolution

The Jiaojia and Sizhuang gold deposits in the Zhaoyuan-Laizhou belt experienced intense water/rock interaction and precipitated the main mineral assemblages of Jiaodong gold

deposits except for arsenic-rich pyrite, which offer an important theme to evaluate the thermodynamic connection among ore-forming fluid evolution, mineral assemblage evolution and gold deposition. *In situ* δ^{34}S and trace elements of stage II and III pyrites in the Sizhuang gold deposit indicate that the two stage ore-forming fluids belonged to different evolutionary stages from the common source (Hu et al., 2020a). Previous studies have pointed out that the sulfidation and fluid immiscibility were two important mechanisms that facilitated gold precipitation in the Jiaodong gold deposits, both of which consumed reduced sulfur in the main ore-forming fluids (Wang et al., 2015; Xu et al., 2016). Therefore, it is suggested that H_2S loss from the main ore-forming fluids (i.e., the decrease of total sulfur concentration, $\sum S_{total}$) could induce the gold deposition coupling with the precipitation of pyrrhotite or magnetite.

Thermodynamic calculations indicate that the oxygen fugacity ($\log fO_2$) upper limit of stability range for pyrrhotite increases from −36.5 to −34.2 when the $\sum S_{total}$ decreases from 0.05 to 0.003 m (Figure 2a–2c). Meanwhile, the stability range of magnetite broadens to more acidic condition, where its stability range expands to a higher ($\log fO_2$<−31.0) and lower oxygen fugacity range when the $\sum S_{total}$ decreases (Figure 2a–2d). Pyrite, pyrrhotite and magnetite can coexist in the low oxygen fugacity and weakly acidic region at appropriate conditions such as the 300°C and $\sum S_{total}$ of 0.003 m (Figure 2c). Moreover, the stability range of chalcopyrite always broadens with the $\sum S_{total}$ decrease (Figure 2a–2d). Therefore, a possible mineral assemblage precipitation process could be predicted at the 300°C, 2000 bar, weak acidity and relatively low oxygen fugacity conditions. Firstly, pyrite and chalcopyrite could precipitate from the H_2S-dominated ore-forming fluid. Secondly, pyrite, chalcopyrite and pyrrhotite could coprecipitate when the H_2S in main ore-forming fluid is continuously consumed by pyrite deposition or fluid immiscibility with the $\log fO_2$ upper limit of stability range for pyrrhotite increasing. Hereafter, the continuous H_2S loss resulted in further decrease of $\sum S_{total}$, which facilitated the coprecipitation of chalcopyrite, pyrrhotite and magnetite assemblage. Lastly, the magnetite and chalcopyrite could coexist and replace previous pyrite due to the exceeding poor sulfur in fluid.

Considering the possibility of the above predicted tendency of mineral assemblages, Hu et al. (2020a) suggested that the evolution of mineral assemblages in the Sizhuang gold deposit was controlled by continuous loss of H_2S from ore-forming fluids that were derived from the common source based on five lines of geologic evidence. Firstly, the $\log fO_2$-pH range of ore-forming fluids in the Sizhuang gold deposit could be constrained in a1–d1 (Figure 2a–2d). Secondly, the varied tendency of mineral assemblages in the Sizhuang gold deposit is consistent with the thermodynamic

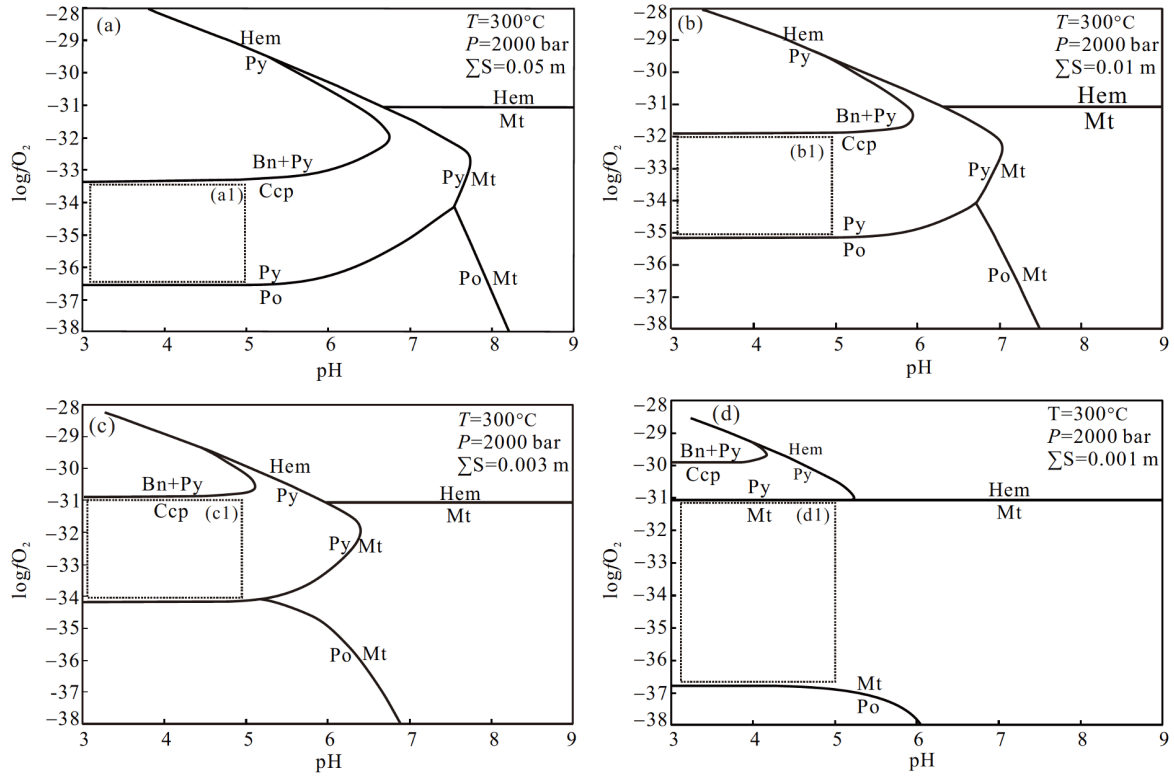

Figure 2 The mineral stability phases at the different $\sum S_{total}$ in Fe-Cu-S-O-H system, (a1)–(d1) are the possible $\log fO_2$-pH range constrained from the mineral assemblages in the Sizhuang gold deposit (Hu et al., 2020a). Mineral abbreviations: Bn=bornite, Ccp=chalcopyrite, Hem=hematite, Mt=magnetite, Po=pyrrhotite, Py=pyrite.

calculation results. Thirdly, the sulfidation with fixation of reduced sulfur and fluid immiscibility occurred widespread (Wei et al., 2015), which possibly resulted in H_2S loss from the main ore-forming fluid or lead the H_2S to enter into gas phase (Naden and Shepherd, 1989). Fourthly, temperature decrease of stage III could facilitate precipitation of chalcopyrite, galena and sphalerite at the constant acidity condition that was buffered by CO_2 (Reed and Palandri, 2006; Xu et al., 2016), where the reduced sulfur in ore-forming fluid could be further fixed by polymetallic sulfides. Lastly, siderite was the main mineral during late stage III fluid which likely possessed sulfur-poor characteristic. Under the circumstance, the existent of CO_2 could lead pyrite to be replaced to form siderite with the release of reduced sulfur into residual fluid according to the Le Chatelier's principle (Hu et al., 2020a). Through the above thermodynamic considerations and geological features, it is suggested that the evolution of mineral assemblages from stage II to III in the Sizhuang gold deposit was controlled by continuous H_2S loss of the main ore-forming fluids that shared the common source.

3.2 Thermodynamic mechanism of gold deposition

The decrease of $\sum S_{total}$ from 0.05 to 0.001 m (about 50 times decrease) could reduce the gold solubility by 2–3 orders of magnitude (a1–d1 in Figure 3a–3d), where it corresponds to the stability ranges where variation for pyrite, pyrrhotite, magnetite and chalcopyrite could occur (a1–d1 in Figure 2a1–d1). Therefore, the $\sum S_{total}$ decrease cannot only be the high-efficiency precipitation mechanism for gold, but also can induce the deposition of pyrrhotite, magnetite and other minerals.

The extensive sulfidation reduced the H_2S concentration and gold solubility of stage II and the early stage III ore-forming fluids in the Sizhuang gold deposit. Therefore, the sulfidation must have been one of critical precipitation mechanisms for gold mineralization. The fluid immiscibility could also facilitate H_2S to enter into gas phase that reduced H_2S concentration of the main ore-forming fluids and led to gold deposition (Naden and Shepherd, 1989; Wei et al., 2015). Based on the widespread pyrite precipitation and fluid immiscibility in the Sizhuang gold deposit, it is suggested that the continuous H_2S loss of the main ore-forming fluids resulted in the precipitation of pyrrhotite and magnetite when it facilitated the rapidly gold deposition. The above evolution of mineral assemblages could be also applied to the Jiaodong gold deposits and other deposits that possess similar thermodynamic conditions.

The other two physicochemical paths to induce gold precipitation are shown as P1 and P2 in Figure 3a. P1 occurs in very oxidizing condition where the dominated mineral assemblage is hematite-magnetite-barite but without pyrrhotite. The precipitation of pyrrhotite in the Sizhuang gold deposit excludes oxidation as the gold deposition mechanism. P2 occurs in low oxidizing environment where the oxygen fugacity decrease facilitates gold precipitation. This physicochemical path for gold precipitation was suitable for the Sanshandao gold deposit where the CH_4-rich ore-forming fluid could be observed in mineralization process (Fan et al., 2003; Li et al., 2013). However, this path cannot be applied to the Sizhuang gold deposit due to the lack of CH_4 in ore-forming fluids (Wei et al., 2015). In addition, cooling can indirectly control gold deposition, because it can not only induce destabilization of metal complexes in ore-forming fluids, but also facilitate fluid immiscibility (Diamond, 2001; Stefánsson and Seward, 2004).

4. Implication of fluid immiscibility and quartz solubility for gold mineralization in the H_2O-NaCl-CO_2 system

Previous studies have shown that physico-chemical properties of ore-forming fluids in the Jiaodong gold deposits are comparable to that of orogenic gold deposits, which are dominated by H_2O-NaCl-CO_2±CH_4 fluids with multiple low-mediate temperature (200–400°C), low salinity (0–10 wt.% NaCl eq.) and high CO_2 contents (4–25 mol.%) (Ridley and Diamond, 2000; Fan et al., 2003; Groves et al., 2003; Bodnar et al., 2014). Various types of auriferous quartz±sulfide ±carbonate veins with complex textures formed as a result of multiple hydrothermal events. In these gold deposits, three types of fluid inclusions are commonly distinguished, including CO_2-rich (>90 mol.% CO_2, type I), H_2O-NaCl-CO_2 (50–80 mol.% CO_2, type IIa; 5–30 mol.% CO_2, type IIb) and low-salinity H_2O-NaCl (type III) inclusions. Distinct types of fluid inclusions with diverse CO_2 contents but similar total homogeneous temperatures were found in the same growth zones of quartz from the Jiaodong gold deposits, suggesting fluid immiscibility during entrapment (Wen et al., 2015). The formation mechanism for various compositional types of fluid inclusions, and the triggers for widespread fluid immiscibility in the Jiaodong gold deposits require to be emphasized, which are critical to the understanding of ore-forming fluid evolution and mineralization processes. In addition, gold mineralization in the Jiaodong gold deposits is intimately related to large-scale silicified alteration and quartz veins, where orebodies are hosted. The precipitation of gold and quartz grains were nearly simultaneous. Therefore, analysis of the dissolution-precipitation behavior of quartz in hydrothermal fluids is important. It can strengthen our understanding of the formation processes of quartz veins, and constrain the corresponding conditions of gold mineralization.

Several thermodynamic modeling calculations have been

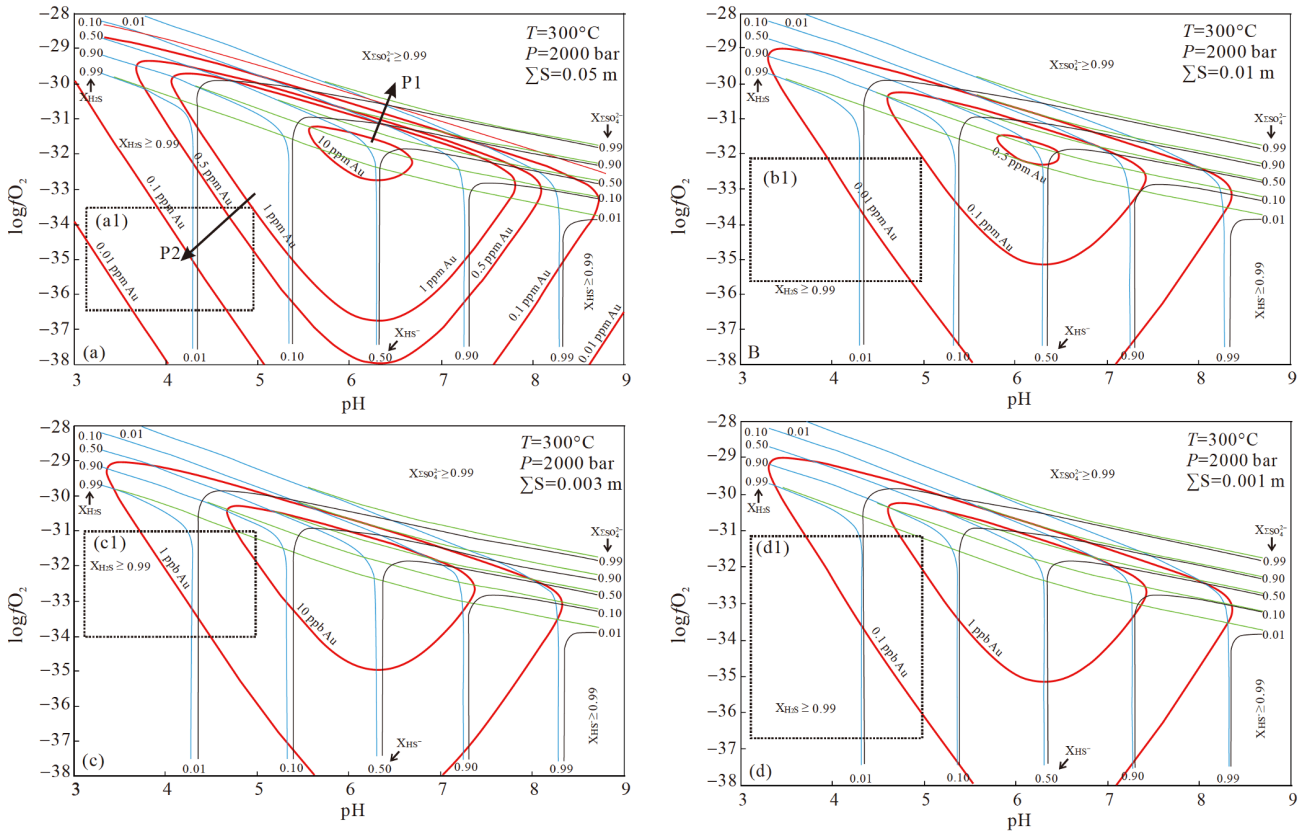

Figure 3 Mole fraction of aqueous sulfur species relative to the total sulfur concentration and the overprinted gold solubility isogram at different $\sum S_{total}$ in log$f$O$_2$-pH diagram. Black boxes (a1)–(d1) represent the possible log$f$O$_2$-pH area of gold precipitation process according to mineral assemblage. (a1)–(d1) correspond to those in Figure 2a–2d, respectively. P1 represents the oxygen fugacity increase path for gold solubility decrease. P2 indicates the oxygen fugacity increase with pH decrease path for the gold solubility decrease (Hu et al., 2020a). 1 ppm=1 μg g^{-1}.

conducted to address the above issues, in a first approximation, mainly based on unary system H_2O, and binary systems such as H_2O-NaCl and H_2O-CO_2 (Anderko and Pitzer, 1993; Driesner and Heinrich, 2007; Mao et al., 2015). Equation of State (EoS) for the H_2O-NaCl-CO_2 ternary system have been developed in the recent decades (Duan et al., 1995; Gottschalk, 2007; Steele-MacInnis, 2018), promoting Li et al. (2020) to characterize phase equilibria, fluid density, and contents of CO_2 and NaCl in liquid and vapor phases at distinct *PVTx* conditions (300–500°C, 0.001–3.5 kbar, 0–4 mol.% NaCl, and 0–20 mol.% CO_2). The types of expected H_2O-NaCl-CO_2 fluid inclusions (Figure 4), triggers for fluid immiscibility, and behavior of quartz dissolution-precipitation (Figure 5) in the orogenic gold system were successfully discussed.

The study of Li et al. (2020) led to several findings as follows: (1) The position and shape of the solvus line, which separates the L+V field from the single-phase fluid region, are affected by CO_2 contents, that is, with increasing CO_2, the position of the solvus shifts to higher temperature and pressure, resulting in the expansion of the L+V field, thus exerting control on the fluid immiscibility. (2) Fluid immiscibility can be triggered by both decompression and cooling, in which paths different types of fluid inclusions are entrapped. Decompression is an efficient mechanism driving fluid immiscibility, producing liquid-rich fluid inclusions with relatively high salinity and vapor-rich inclusions with relatively low CO_2 contents (type IIb). In contrast, a variety of fluid inclusion types, including liquid-rich inclusions with low salinity and low CO_2 contents (type IIb), and vapor-rich inclusions with moderate-high CO_2 contents (up to ~65 mol.%, type IIa) (Figure 4). In contrast to coeval fluid inclusion types entrapped during fluid immiscibility, fluid inclusion assemblages (FIA) with low CO_2 contents (type IIb) are more common in gold mineralization systems, representing entrapment of sing-phase ore-forming fluids. (3) The referred "pure CO_2" fluid inclusions, which are often observed in Jiaodong and other orogenic gold deposits, cannot be produced by phase separation under reasonable *PTx* conditions for orogenic mineralization. Inclusions of this type may be the result of decrepitation of primary H_2O-NaCl-CO_2 fluid inclusions. Fluid immiscibility is a significant mechanism of large-scale gold precipitation in the Jiaodong gold deposits (Fan et al., 2003; Li et al., 2018b). By analyzing the coexisting fluid inclusion types, we can obtain information on the triggers of fluid immiscibility, and further to investigate the

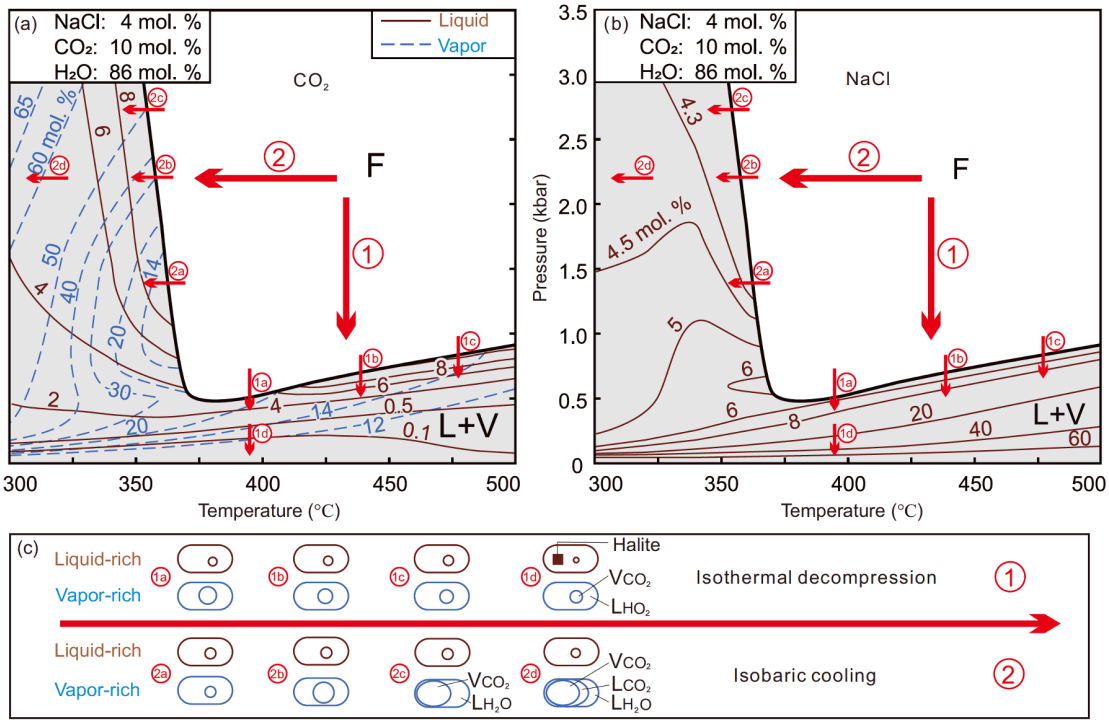

Figure 4 Isothermal decompression and isobaric cooling paths of H_2O-NaCl-CO_2 fluids, after Li et al. (2020). (a) CO_2 contents in the L+V field. (b) NaCl contents in the L+V field. (c) Distinct types of fluid inclusions at room temperature entrapped during fluid decompression and cooling.

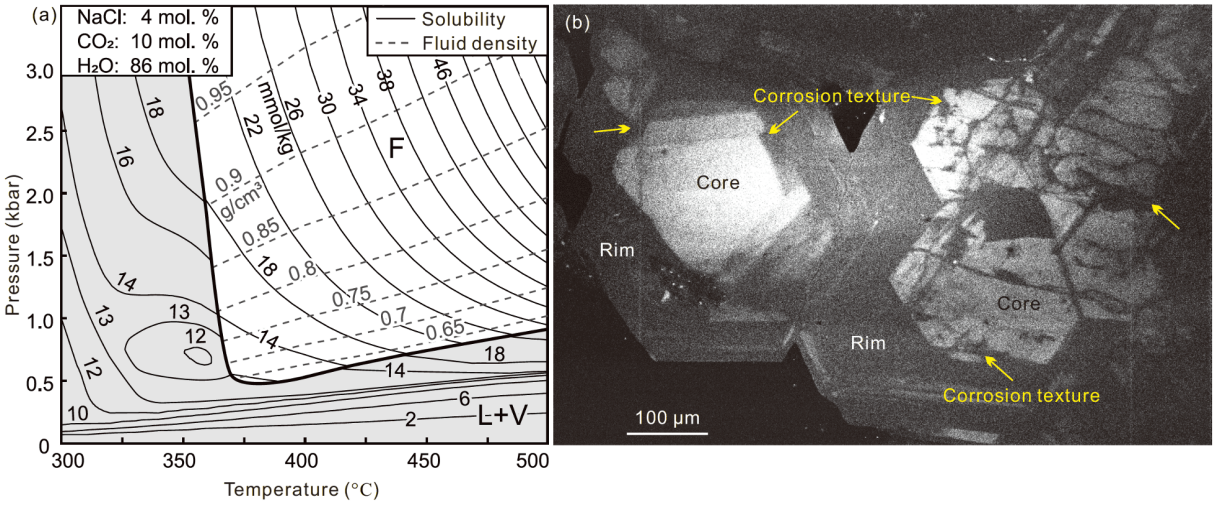

Figure 5 (a) Quartz solubility isopleths in H_2O-NaCl-CO_2 fluids, after Li et al. (2020). (b) Cathodoluminescence images of quartz grains from the quartz-sulfide veins in the Majiayao gold deposit in Jiaodong, showing complex zoning and corrosion texture.

changes of physico-chemical conditions of ore-forming fluids and the corresponding conditions of gold mineralization in the Jiaodong gold deposits.

Based on phase diagrams constructed by thermodynamic modeling of the H_2O-NaCl-CO_2 ternary system, Li et al. (2020) built quartz solubility model using the equation by Brooks and Steele-MacInnis (2019) for H_2O-NaCl-CO_2 system (Figure 5). The quartz solubility model is of great significance to discuss the formation of quartz veins and the micro-structure of quartz in Jiaodong gold deposits. The quartz solubility in H_2O-NaCl-CO_2 fluids shows strong dependence on temperature, pressure, and CO_2 content. It generally decreases with decreasing temperature and pressure, and increasing CO_2 content both in the single- and two-phase fluids, but exhibits retrograde behavior in the L+V field and near the phase boundary between single-phase and L+V fields (Figure 5a). The retrograde quartz solubility can result in corrosion textures between quartz cores and rims (Figure 5b). The quartz solubility depends strongly on temperature at high pressure (Figure 5a), whereas it depends

strongly on pressure at high temperature. The solubility model can be used to discuss behavior of quartz dissolution-precipitation and formation of distinct quartz veins in orogenic gold deposits. The formation of bedding-parallel shear veins is controlled by decompression-induced quartz precipitation during pressure fluctuation. In contrast, fault-related extensional veins are associated with initial decompression-induced quartz precipitation and subsequent cooling-dominated deposition. Due to distinct paths of hydrothermal fluids, there are differences of fluid inclusions between the two-type quartz veins. Two styles of gold mineralization, disseminated sulfide replacement and quart-sulfide vein-type mineralization, in Jiaodong gold deposits are produced in distinct host structures, where conditions of quartz deposition are different, thus forming diverse types of quartz veins. As a result of multistage hydrothermal events and change of quartz solubility, quartz grains commonly show complex zoning and corrosion texture, representing the behavior of dissolution and reprecipitation (Figure 5b).

5. Pyrite precipitation and implication for the gold ore-forming processes

Pyrite is the most ubiquitous and significant gold-bearing sulfide mineral from early to late mineralization stages in Jiaodong gold deposits. Its micro-textures, trace elements and isotopic composition characteristics help to clarify the complex crystallization histories of pyrite, reveal the sources and evolutions of ore metals, and understand precipitation mechanisms of gold mineralization (Reich et al., 2005; Large et al., 2009; Kusebauch et al., 2019; Wu et al., 2019a). Generally, the euhedral and pristine pyrite crystals/aggregates without many pores and mineral inclusions suggest that they were precipitated under relatively stable physicochemical conditions with approximately constant chemical compositions, pH and oxygen fugacity (Large et al., 2009; Román et al., 2019). The anhedral to euhedral, porous or zoned pyrite grains/aggregates with abundant micro- to nano-mineral inclusions (mainly galena, sphalerite, and chalcopyrite) may indicate rapid crystallization processes under rapidly cooling or other abruptly change of fluid compositions and physicochemical conditions, which could be triggered by the vigorous boiling or immiscibility of ore-forming fluids or cycled involvement of external fluids (Williams-Jones and Heinrich, 2005; Peterson and Mavrogenes, 2014; Wu et al., 2019a).

5.1 Invisible gold mineralization related with arsenian pyrite

Generally, gold mineralization in the Jiaodong deposits is dominated by independent visible native gold or electrum grains (Mills et al., 2015a; Zhu et al., 2015; Yang et al., 2016), occurring within fractures or as inclusions in pyrite. However, there are few detailed studies which investigated the gold concentrations and occurrences with respective to the host pyrite. The pyrites from Xincheng, Xiadian and Wang'ershan altered rock type Au deposits usually have no complex internal textures (Mills et al., 2015a; Yang et al., 2016; Hu et al., 2020b). The results of LA-ICP-MS *in-situ* trace elements indicated the very low concentrations of arsenic (<1000 ppm) and lattice gold (<1 ppm), and a potential occurrence of gold nanoparticles locally in those pyrites. However, other ore-related pyrites from several high-grade vein type Au deposits in the central Penglai-Qixia belt and the eastern Muping-Rushan belt showed complex micro-textures with regular variations of trace elements (the coupled As-Au-rich zoning) and sulfur isotopes compositions at individual grain-scales, implying the complex ore-forming fluid activities (Feng et al., 2018, 2020; Li et al., 2018b; Zhang Y W et al., 2020). These pyrites generally possess As-poor dark core domains (similar to the above-mentioned As-poor pyrites from altered rock type Au deposits) and As-rich bright zoned rim domains (As contents up to 2–3%, Feng et al., 2018, 2020; Li et al., 2018b; Zhang Y W et al., 2020), which are usually intergrown with polymetallic sulfides, such as galena, sphalerite, chalcopyrite and arsenopyrite (Figure 6a, 6b).

The recent results of LA-ICP-MS *in-situ* trace elements and Nano-SIMS mapping analyses indicated that the rim domains of pyrite have obvious higher As-Au concentrations and $\delta^{34}S$ values than core domains (Figure 6c, 6d), showing positive correlations among them (Feng et al., 2018, 2020; Li et al., 2018b; Fan et al., 2018; Zhang Y W et al., 2020), which are also consistent with the coupled behaviors between As and Au within those arsenian pyrite from Carlin-type and orogenic Au deposits (Large et al., 2009). Integrated with the results of *in-situ* pyrite S isotopes, fluid inclusion microthermometry and other stable isotopes, it was proposed that these As-rich fluids may be caused by the interactions between initial ore fluids and As-rich meta-sedimentary rocks, such as regional Paleoproterozoic Fenzishan and Jingshan groups, Neoproterozoic Penglai group (Feng et al., 2018). The deep-cycled meteoric water might have also contributed to the ore-forming systems (Zhang Y W et al., 2020). The oscillatory zoning of As-Au was interpreted to be the result of pressure fluctuation and repeated local fluid phase separation around the pyrite crystal (Li et al., 2018b).

It has been demonstrated that Au is preferentially concentrated in As-rich pyrite as "invisible gold" (solid solution (Au^{+}) or nanoparticles (Au^{0})) and As usually occur as As^{-} substituting for S^{-} in the pyrite lattice (Mikhlin et al., 2011). The crystal nature of pyrite could be changed because of the As substitution for S, leading to the easy gathering of Au onto the reduced growing surface of As-bearing pyrite via

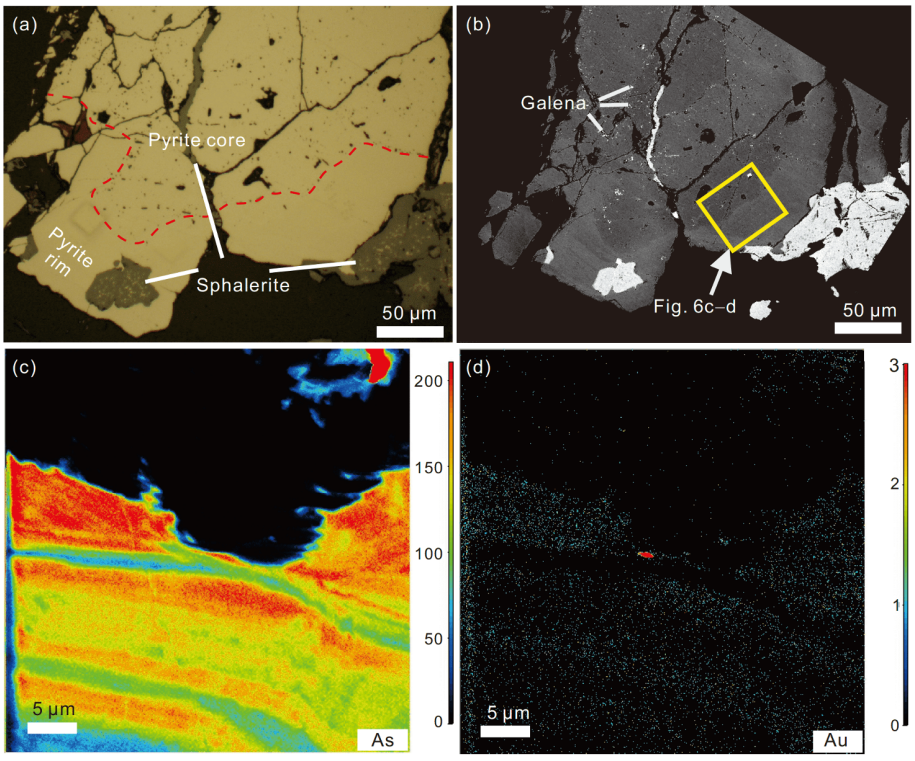

Figure 6 The ore-related pyrite with complex textures in the Muping gold deposit ((a)–(b)); the Nano-SIMS mappings of As and Au ((c)–(d)).

chemisorption mechanism, or the direct incorporation of Au into the vacancies, defects and octahedral positions of pyrite crystal structure (Palenik et al., 2004; Kusebauch et al., 2019; Xing et al., 2019). All the above processes would result in a very high Au partition coefficient between fluid and pyrite during ore fluids precipitation (Kusebauch et al., 2019). Thus, it was interpreted that the formation of Au-As rich pyrite rims was mainly controlled by As concentrations of ore-forming fluids and the accumulation of invisible gold within As-rich pyrite rims is likely to be a passive response. In addition, petrographic observations also suggest that these As-rich pyrites have a close spatial-temporal relationship with abundant visible gold grains, which are significant for the formation of high-grade ores. Many As-bearing minerals (e.g., arsenopyrites, tetrahedrite) and As-rich pyrite have been documented in the Sanshandao, Denggezhuang and some other deposits (Hu et al., 2006, 2013; Mills et al., 2015a; Wen et al., 2016; Fan et al., 2018; Peng et al., 2021). It is suggested that widespread gold mineralizing events correlated with the As element, which may be an indicator for the future exploration of high-grade gold ores in the Jiaodong province.

5.2 The formation and precipitation mechanisms of "visible gold"

Gold mineralization in both the vein-type and altered rock-type Au deposits in Jiaodong is dominated by visible native gold and/or electrum grains. Such visible gold could be directly precipitated from over-saturation fluids, or be formed by the mobilization of As and Au expelled from early-formed pyrite lattice and local enrichment via fluid-assisted replacements (termed as coupled dissolution-reprecipitation) (Large et al., 2009; Cook et al., 2013). Most pyrite grains from the altered rock-type Au deposits have low concentrations of As and scarcely contain invisible gold within internal crystal lattices, whereas As-rich pyrite from vein-type deposits generally formed later than or contemporaneously with visible gold grains (Feng et al., 2018; Zhang Y W et al., 2020). Considering the extremely limited Au and As contents in earlier pyrite cores and the principle of mass balance, there are not enough metallogenic materials for the formation of late-stage visible gold, despite of the intense corrosion and replacement of earlier cores. Therefore, it is most likely that the visible gold mineralization in the Jiaodong deposits is directly precipitated from ore-forming fluid under the Au over-saturation condition, rather than the dissolution and reprecipitation of earlier pyrite.

Previous studies have shown that the gold mineralization (visible or invisible gold) and ore grades are mainly controlled by the As contents and total S contents of ore-forming fluids in Carlin-type gold deposits (Kusebauch et al., 2019). The As-rich pyrite precipitation could scavenge plenty of dissolved gold from hydrothermal solution, making it not

easy for the over-saturation of gold and the subsequently formation of visible gold via the pyritization processes. This is also why the primary gold mineralization occurs mainly as the form of invisible gold and appearance of late-stage visible gold generally results from the fluid-assisted remobilization of earlier pyrite with high invisible gold content in many Carlin-type and orogenic gold deposits (Large et al., 2009; Cook et al., 2013; Kusebauch et al., 2019), rather than direct precipitation from ore-forming fluids. The results of *in-situ* trace elements showed that the average As concentrations of pyrite from Jiaodong gold deposits, even for quartz vein-type deposits with relatively higher As contents, are obviously lower by several magnitudes than those from Carlin-type and orogenic gold deposits (Su et al., 2012; Yang et al., 2016; Feng et al., 2018; Zhang Y W et al., 2020). Therefore, the Jiaodong pyrite could not efficiently scavenge the gold from ore fluids into crystal structures. With the deposition of sulfide minerals, the continuous loss of total sulfur contents in hydrothermal fluids may be a key factor controlling the gold over-saturation precipitation in Jiaodong deposit.

Compared to quartz vein-type Au deposits, the pyrite from pyrite-sericite-quartz alteration zones in altered rock-type deposits is characterized by euhedral crystals, Au-As depletions and various S isotopic compositions (Feng et al., 2018, 2020; Hu et al., 2020b; Zhang Y W et al., 2020; Peng et al., 2021), which could be related with the different environments and evolutions of ore-forming fluids. Generally, the quartz vein-type deposits are formed by the more intense dilation induced by torsional stresses block rotation and abrupt decompression. Within such relatively open ore-forming system, the intense fluid immiscibility may be triggered by involvement of external fluids and the pressure fluctuations (Figure 7), leading to the abrupt change of fluid physicochemical conditions and compositions and subsequent precipitation of zoned, arsenic-rich, pores-rich and mineral inclusions-rich pyrite (Li et al., 2018b; Feng et al., 2018, 2020; Zhang Y W et al., 2020; Peng et al., 2021). In contrast, the altered rock-type deposits are mainly formed under the condition of the transpression structure environment and the relatively closed ore-forming systems in the main fault zones, resulting in large-scale alteration and mineralization (e.g., fluid/rock interactions and sulfidations), and relatively gentle evolution of the fluid compositions and physicochemical conditions. Even though ore fluids experienced immiscibility during mineralized stages, it was also a gentle evolution process with more gradual cooling and decompression (Hu et al., 2020b).

6. Control of metallogenic mechanism on visible gold fineness

Visible gold, also called native gold, electrum and kustelite, is an important gold mineralization type in different types of gold deposits, and is a main kind of gold resource. The visible gold grain can be defined as individual crystals with grain size at micrometer level that can be observed under scanning electron microscope, optical microscope, and even from hand specimen, which is different from "invisible gold" occurring as lattice gold or nanoparticle gold hosted in other minerals. Gold grain can incorporate various elements, in which Ag is in complete solid solution with Au, and consequently, gold grains can have high and highly variable content of Ag (Gammons and Williams-Jones, 1995; Pal'yanova, 2008). The Ag content of gold grain is commonly expressed as gold fineness, which is calculated by 1000× wt% Au/(wt% Au+wt% Ag) (Hough et al., 2009).

Previous statistical data of gold fineness of different gold deposits showed that different gold deposits had different ranges of gold fineness, and its values seemed to be related to formation depth of deposits. Fisher (1945) found that hypozonal hydrothermal gold deposits had gold fineness ranging from 800 to 1000, whereas those epizonal ones varied from 500 to 800. Morrison et al. (1991) pointed out that different gold deposits showed different ranges with respect to gold fineness, and as a whole, the hypozonal deposits (like Precambrian orogenic gold deposits) had high and concentrated gold fineness (800–1000), whereas those epithermal ones were characterized by low but variable gold fineness (concentrated at 400–1000).

6.1 Tempo-spatial evolution of visible gold fineness

The disseminated-type and quartz vein-type gold deposits in Jiaodong are both characterized by visible gold mineralization, in which visible gold grains mainly occur in interior, grain boundaries and fractures of pyrite and sulfide minerals (Yang et al., 2016; Li et al., 2018b; Feng et al., 2018; Peng et al., 2021). Preliminary compilation of data on the gold fineness of Jiaodong gold deposits from Meng et al. (1998) show relatively low values concentrated at 550 to 750, which indicates a shallow formation depth for Jiaodong gold deposits. From a further evaluation of the data, it can be seen that the disseminated-type and quartz vein-type gold deposits in Jiaodong have different gold fineness ranges. The disseminated gold deposits, such as Jiehe and Dujiaya, are characterized by high gold fineness (>900). However, the quartz vein-type deposits of Heilangou, Linglong, Sanjia and Jinqingding show relatively low gold fineness (600–800). Recent studies are also in favor of the gold fineness difference between the two types of deposits. The typical disseminated gold deposit of Jiajiao is characterized by high gold fineness, corresponding to native gold (>800; Hu and Fan, 2018), whereas quartz vein type deposits, like Zhuangzi and Heilangou, show relatively low gold fineness, predominantly being electrum (<800; Feng et al., 2018; Li et al.,

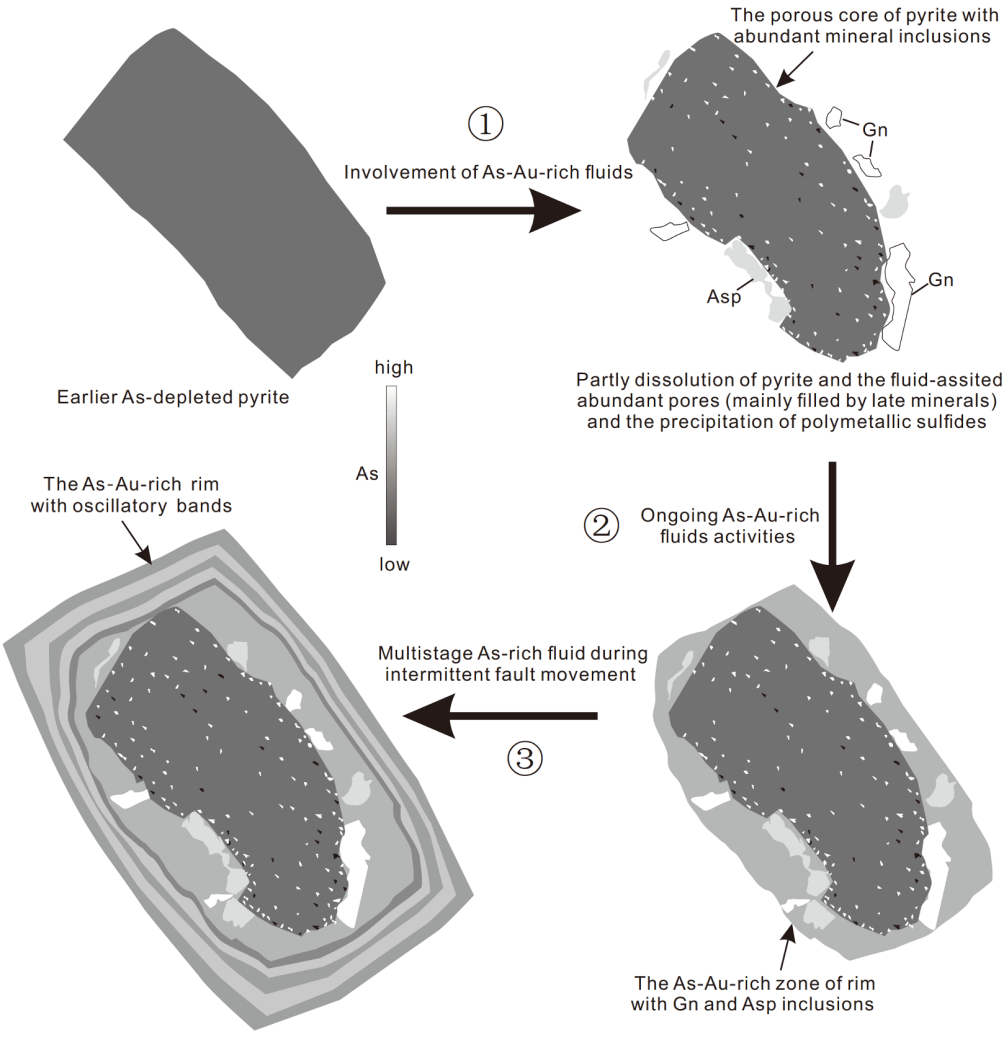

Figure 7 The sketch map illustrating formation of pyrite in the Heilan'gou gold deposit.

2018b).

In addition to the gold fineness difference between the two types of gold deposits in Jiaodong, there is also gold fineness variation in individual gold deposits of Jiaodong. It is noticed that in addition to high gold fineness (Hu and Fan, 2018), low gold fineness was also reported in the Jiaojia deposit (<800; Meng et al., 1998). Mills et al. (2015b) also found that the steeply dipping No. III ore body in Jiaojia (quartz vein-type mineralization) was characterized by Ag-rich mineralization, distinct from the disseminated-type main ore bodies. Besides, from the deep to shallow region, the ratio of Au/Ag tends to decrease in the deposit (Sun et al., 2020). These features all suggest temporal and spatial evolution of gold fineness in the Jiaojia gold deposit. A stage of Ag-mineralization, characterized by deposition of kustelite and argentite, is developed after the gold mineralization in Dayingezhuang gold deposit, which is also indicative of temporal evolution of gold fineness and Au-Ag mineralization (Yuan et al., 2019). Besides, although electrum is dominantly occurring in the Xincheng gold deposit, the relative content between Au and Ag in visible gold grains varies greatly (Yang et al., 2016), also implying possible variations of gold fineness among different stages of mineralization in the deposit. These studies all indicate a common temporal and spatial evolution of gold fineness in the gold deposits of Jiaodong, which may be correlated with the tempo-spatial evolution of ore-forming fluid and mineralization.

6.2 Control on tempo-spatial evolution of gold fineness in the Sanshandao gold deposit

The Sanshandao, one of the largest disseminated gold deposits in Jiaodong (Fan et al., 2003), is characterized by the occurrence of arsenopyrite, which implies the existence of As-rich quartz vein-type mineralization (Feng et al., 2018; Li et al., 2018b). Recently, a series of drill holes deep to 400.17 m have been established, from which it was revealed

that the gold mineralization extended to 2000 m depth (Wen et al., 2016), which provides an excellent site to investigate the integrated temporal and spatial evolution of gold fineness and gold mineralization.

The Sanshandao gold deposit shows two generations of gold mineralization (Peng et al., 2021). The early generation is represented by beresitization and quartz-pyrite vein, in which visible gold grains are associated with early pyrites, whereas the late generation is represented by quartz-polysulfide vein, in which visible gold grains are intergrown with late pyrite, arsenopyrite, galena, chalcopyrite and sphalerite (Figure 8). According to the detailed investigations for the drill holes, the early gold mineralization extends to 2700 m depth, whereas the late gold mineralization is concentrated at shallow region, with the deepest sample occurring at ca. 1450 m depth.

In-situ trace element analyses of pyrite show that the early pyrites are homogeneous in texture, and are characterized by enrichment of Co, Ni and Bi, and depletion of As and Au. In addition, with decreasing depth, the concentrations of Co and Ni decrease, whereas the concentrations of As show increasing tendency. The late pyrites, the "rim" pyrite formed by replacement of early pyrite, are characterized by depletion of Co, Ni and Bi, and enrichment of As and Au. The textural and trace elemental features of pyrites suggest that, in the two generations of gold mineralization with distinct mineralized style and mineral assemblages, fluid/rock interaction (sulfidation) is the mechanism of the early gold mineralization, whereas decompression and phase separation of fluid at shallow depth is the mechanism of the late gold mineralization (Peng et al., 2021).

Regarding gold fineness, the early gold generation has high gold fineness (729–961), which decreases from 870 (average value) at 2650 m depth to 752 at 420 m depth, whereas the late gold generation is characterized by markedly low gold fineness (218–719) (Figure 9). The ore-forming fluids of the Sanshandao gold deposit are weakly acidic, and reduced fluids (Fan et al., 2003; Hu et al., 2013; Li et al., 2013), and hence, in the fluid migration process, Au is complexed with S, whereas Ag is complexed with Cl (Morrison et al., 1991; Pal'yanova, 2008). Under the fluid/rock interaction background of the early gold generation, pyrite deposition and consequent consumption of S in fluids would result in the destabilization of the Au-S complex, but have limited influence on the Ag-Cl complex, contributing to gold mineralization with relatively high gold fineness. In the fluid migrating process with decreasing depth, temperature (pressure) of the ore-forming fluids decreased, and fluid/rock interaction (+fluid reduction) was enhanced, which led to successive decrease of gold fineness. However, under the decompression and phase separation of ore-forming fluids background, the Au-S and Ag-Cl complexes in the ore-forming fluid would markedly destabilize, contributing to low gold fineness of the late gold generation, and at the same time, other ore elements in the fluids would precipitate to form the polysulfide mineral assemblage.

In the Sanshandao gold deposit, gold fineness, mineral assemblage, and textural and chemical features of sulfide minerals display coupled temporal and spatial evolutions, which show the control on the gold fineness from metallogenic mechanism, and also demonstrate that variation of gold fineness is closely related to the temporal and spatial evo-

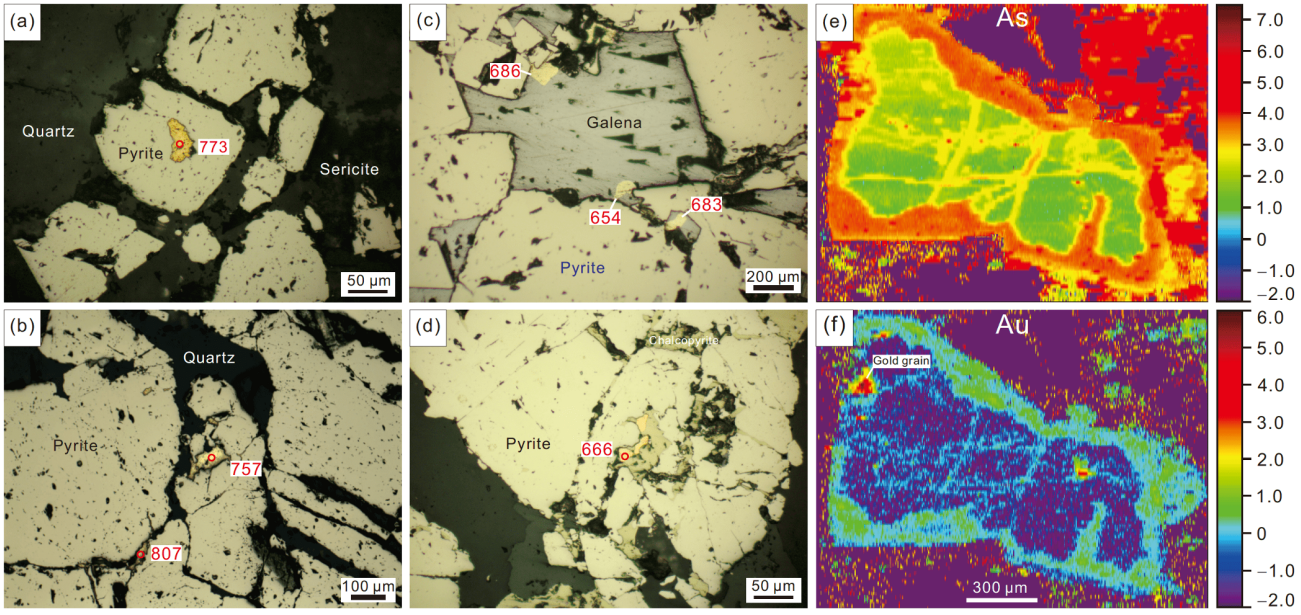

Figure 8 Mineral assemblage and visible gold in the different gold generations of the Sanshandao gold deposit. (a) Beresitization; (b) quartz-pyrite vein; (c)–(d) quartz-polysulfide vein, visible gold grains are intergrown with galena and chalcopyrite, respectively; (e)–(f) As and Au LA-ICP-MS mapping of late pyrite, concentration scales are in ppm at logarithmic 10.

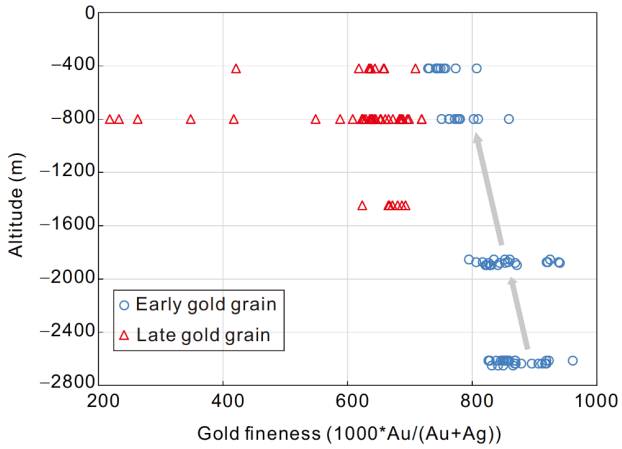

Figure 9 (Color online) Spatio-temporal variations of gold fineness of the Sanshandao gold deposit.

lution of gold mineralization.

7. Implications for the genesis of the Jiaodong gold deposits

Based on the studies described above on Au deposition, the transportation mechanism of Au can be well constrained. Although the results were obtained from the representative Jiaodong gold deposits, the conclusions could be suitable for the other gold deposits in the Jiaodong province. The Jiaodong gold deposits commonly have the mineral assemblages of sulfide+quartz throughout the hydrothermal evolution, which imply that sulfur was ubiquitous and mainly presented as reduced species (such as H_2S/HS^-) in the fluids. In combination with the fluid inclusions dominantly composed by H_2O-CO_2-NaCl, the original ore-forming fluids of the Jiaodong gold deposits is inferred to be H_2S-bearing H_2O-CO_2-NaCl fluids. According to the PTX-pH properties of the H_2O-CO_2-NaCl fluid system (Li and Duan, 2007), the pH values of the above fluids in the early stage are estimated to be 3–4. Numerous studies have shown that in the moderate- to low-temperature, low-salinity, weakly acidic to alkaline and reduced S-bearing hydrothermal fluids the Au is mainly transported as hydrogen sulfide species (e.g., $Au(HS)_2^-$, Pokrovski et al., 2014; Trigub et al., 2017). This might be the major mode of transport for Au in the Jiaodong gold deposits. However, the above conventional transportation of Au is neither the only way nor the perfect one to explain the "gold-only" feature as well as the highly concentrated deposition of the Jiaodong gold deposits. In recent years, more and more evidence show that S_3^- can form very stable and soluble complexes with Au^+ (e.g., $Au(HS)S_3$) in aqueous solutions at the conditions of elevated temperature, pressure and sulfur concentration (e.g., >350°C, >500 bar, >0.5 wt% S), acidic-to-neutral pH and oxygen fugacity of H_2S-SO_2 coexistence, and its abundance is 10–1000 times more than the HS^- with comparable strength for Au^+ (Pokrovski and Dubrovinsky, 2015). The physicochemical conditions of the auriferous fluids in the Jiaodong gold deposits generally match with those required for the Au^+-S_3^- complexes, suggesting that the presence of Au^+-S_3^- complexes might occur. Further studies are thus required to test the presence of S_3^- in the Jiaodong gold deposits. Colloidal particle has also been proposed as an important medium to transport Au in hydrothermal fluids (e.g., Herrington and Wilkinson, 1993; Saunders and Burke, 2017). In that case, the gold colloids are commonly assisted by silica colloids for the stability in the fluids and thus co-precipitate with amorphous silica or quartz, and the nanoparticles of gold commonly aggregate to form fractal dendrites (Saunders and Burke, 2017). These phenomena, however, were not identified in the Jiaodong gold deposits.

Detailed studies on *in-situ* trace elemental and S isotopic compositions of pyrite from some of the representative Jiaodong gold deposits (e.g., Wang'ershan, Linglong, Xiadian, Heilangou, Zhuangzi, Jiangjiayao and Denggezhuang gold deposits) have been conducted recently (Li et al., 2018b; Feng et al., 2018; Hu et al., 2020b; Zhang Y W et al., 2020). These studies reveal three interesting trends as follows: (1) low-δ^{34}S (e.g., low to 4‰) and high-δ^{34}S (e.g., high up to 20‰) values coexist in one deposit or even in one pyrite grain; (2) the Jiaojia-style mineralization show relatively higher δ^{34}S values than those of the Linglong-style mineralization in one metallogenetic belt; (3) the increase of δ^{34}S is accompanied by the increase of As and Au. Because of the simple mineral assemblages without significant change in oxygen fugacity, the coexistence of low- and high-δ^{34}S values could not have been induced by isotopic fractionation, but more likely resulted from different sources. The low δ^{34}S values are close to those of the coeval intermediate-mafic dykes. Combined with many other isotopes (e.g., C-O-Sr-Nd-Pb-He-Ar) showing significant involvements of mantle components in the Jiaodong gold deposits (Li and Santosh, 2014; Wen et al., 2016; Tan et al., 2018), mantle-derived or deeply-sourced fluids seem to play the dominant role for the generation of the Jiaodong gold deposits. The high δ^{34}S values are higher than those of the Mesozoic mafic dykes (mean of 2.4–6.9‰), granitoids (mean of 6.7–7.7‰) and late Archean metamorphic rocks (0–7.8‰), but close to the regional Paleoproterozoic metasedimentary rocks (8.2–12.0‰) (Wang et al., 2002). In combination with the coupled increase of As and Au, it is likely that the high-δ^{34}S auriferous fluids leached additional S, As and Au from the Precambrian metasedimentary rocks along the pathways.

The higher δ^{34}S values in the Jiaojia-style mineralization

than in the Linglong-style mineralization suggest that fluid-rock interaction could lead to the increase of δ^{34}S. Hydrothermal fluids leaching ore-forming materials from wallrocks have been widely observed in the other gold deposits, such as the Carlin-type gold deposits (Large et al., 2011). The cross-cutting relationships between the low- and high-δ^{34}S zones in a single pyrite grain suggest that the low- and high-δ^{34}S auriferous fluids were mixed at some conditions. The two types of fluids cannot be distinguished by fluid inclusions. Combined with the focused mineralization of the Jiaodong gold deposits, it is inferred that the above fluids were originally derived from a uniform mechanism. One possible way is that the original auriferous fluids were transported along different pathways, some of which underwent little fluid-rock interaction or wallrock contamination and thus kept their primary isotopic compositions. By contrast, the other parts of fluids were subjected to intense fluid-rock interaction or wallrock contamination, leaching additional S, As and Au from the wallrocks. The two types of fluids were finally mixed with each other at favorable locations in the shallow depths.

The above results illustrate that the ore-forming fluids changed during upward transportation, although how the fluids were generated remains unsolved. The Jiaodong gold deposits have long been considered as orogenic gold deposits (Qiu et al., 2002; Goldfarb and Santosh, 2014; Groves et al., 2020) because their ore-forming fluids (e.g., salinities, homogenization temperatures and CO_2 contents) show many similarities to those of the orogenic gold deposits. Systematic studies on *in-situ* (LA-ICP-MS) elemental compositions of fluid inclusions and quartz from the Linglong gold deposit (the most representative gold deposit of Linglong-style mineralization) show that the elemental concentrations and ratios of the ore-forming fluids are more similar to those of the metamorphic fluids derived from high-grade metamorphism (e.g., amphibolite facies), but distinct from those of the Carlin-type and epithermal gold deposits. These results suggest that the auriferous fluids might have been derived from high-grade metamorphism. It has been widely accepted that orogenic gold deposits are generated through dehydration of shallow crustal rocks (sedimentary or volcanic rocks) during greenschist-amphibolite facies metamorphism due to the favorable release of fluids and Au (Tomkins and Grundy, 2009; Phillips and Powell, 2010; Zhong et al., 2015). However, such metamorphism did not occur in the Jiaodong Peninsula during the period of gold mineralization (120±5 Ma) and occurred 2 billion years prior to the gold mineralization in the region. Experimental studies and thermodynamic modeling showed that dehydration of mafic rocks can occur at 500–550°C during amphibolite facies metamorphism, leading to the formation of CO_2-bearing fluids (Elmer et al., 2006; Starr and Pattison, 2019). At even higher-grade metamorphism (amphibolite to granulite facies), CO_2 and brine fluids can be generated (Touret, 2009; Manning, 2018), forming CO_2-rich quartz veins (Fu and Touret, 2014). Actually, orogenic gold deposits generated through high-grade metamorphism (amphibolite to granulite facies) in the lower crust have long been proposed and explained (e.g., Cameron, 1989; Groves, 1993), although there are still some controversies (Phillips and Powell, 2009; Tomkins and Grundy, 2009). Recent studies on gold mobilization during metamorphic devolatilization showed that as much as 59–77% of the initial Au content can be mobilized during progressive metamorphism to upper amphibolite facies conditions (>550°C) (Patten et al., 2020). Magneto-telluric and seismic investigations on crustal structure indicated that there is a thick crust-mantle transitional zone beneath the Jiaodong Peninsula and the crust were subjected to intense extensional stress (Yu et al., 2020), suggesting a remarkable underplating of basaltic magmas at the lower crust of the Jiaodong Peninsula (Zheng et al., 2012; Ping et al., 2019). The mafic underplating is corroborated by the lower crustal xenoliths in the Mesozoic and Cenozoic volcanic rocks from the eastern North China craton (including the Jiaodong Peninsula), which contain numerous zircons with U-Pb ages of 157–114 Ma (Liu et al., 2001; Huang et al., 2004; Ying et al., 2010; Zhang, 2012; Tang et al., 2014). The recent studies on Pb isotopic compositions also support the regional-scale underplating of mafic magmas in the lower crust of the Jiaodong Peninsula (Xiong et al., 2020). Because the lithospheric mantle beneath the eastern North China Craton was metasomatized by the paleo-Pacific oceanic slab during the Mesozoic, the mantle-derived basaltic magmas were relatively enriched in H_2O and Au (Xia et al., 2017; Wang et al., 2019), which could form sulfide-rich Au-bearing mafic accumulates (e.g., amphibole cumulates, Davidson et al., 2007; Hou et al., 2017). Dehydration of these accumulates could occur during subsequent heating by asthenospheric upwelling, forming CO_2-rich auriferous fluids.

Therefore, based on the above results, a metamorphic model for the generation of the Jiaodong gold deposits is proposed. The major ore-forming processes are as follows.

(1) Large-scale mafic underplating occurred at the lower crust of the Jiaodong Peninsula during late Jurassic and early Cretaceous, forming the H_2O- and Au-rich amphibolite cumulates (juvenile lower crust). The Triassic collision between the NCC and the South China Block along the southeastern NCC led to the lithospheric thickening and subsequent thinning (probably through delamination), providing favorable conditions for the underplating of the mafic magmas.

(2) Intense asthenospheric upwelling occurred during 130–120 Ma due to the Pacific plate changing its subduction direction or the rollback of the paleo-Pacific plate, heating the amphibole cumulates to dehydrate (at amphibolite to gran-

ulite facies) and thus resulting in the generation of CO_2-rich auriferous fluids. The auriferous fluids were transported along the deeply-seated faults (such as the Tanlu fault and its secondary faults), forming the fault-controlled gold deposits (Figure 10).

(3) Au was mainly transported as hydrogen sulfide species (e.g., $Au(HS)_2^-$) and finally deposited following fluid boiling and fluid-rock interaction, forming either the Linglong-style or the Jiaojia-style mineralization at different tectonic positions.

8. Conclusion and implication

The terminal effect of mineralization is an important basic element of economic geology. Related research is of important significance to reveal the spatiotemporal evolution and accumulation process of ore-forming fluid, to investigate the occurrence of ore-forming elements and the spatial change of the paragenetic association of elements and minerals, to clarify the evolution of ore-forming system and the constraints on the migration and precipitation of elements, to analyze the control and recognition of fault properties on the spatial positioning and metallogenic types of ore bodies, to distinguish the geochemical barrier of large-scale mineral precipitation, to explore the critical mechanism of massive accumulation of elements, and to propose a reasonable metallogenic model. Based on the evolution of mineral assemblage and the thermodynamic relationship with gold precipitation in Jiaodong typical gold deposits, this paper suggests that the extensive sulfidation and immiscibility of ore-forming fluid resulted in a change of stability domain of mineral phase, and the decrease of total sulfur concentration (the loss of H_2S) in fluid more effectively reduces the solubility of gold. However, more accurate models need to be built to simulate and predict the control of water/rock interaction on the precipitation behavior of metal elements. H_2O-NaCl-CO_2 mixed fluid is very common in magmatic, metamorphic and hydrothermal system, and plays an important role in magmatism and mineralization. Based on the model construction of quartz solubility and the forward calculation of phase behavior of H_2O-NaCl-CO_2 fluid system under different *PVTx* conditions, this paper discusses in detail the control of immiscibility and quartz dissolution precipitation of CO_2 bearing fluid system on gold mineralization, which is of great significant for the discussion of the formation mechanism of different types of fluid inclusions and quartz veins in orogenic and intrusive related gold deposits, as well as the detailed metallogenic process. Pyrite is the main ore mineral and the most important gold bearing mineral in gold deposits. It often shows a complex growth history, and is an important proxy for accurately determining the metal source and the gold precipitation process. This paper discussed the gold occurrence and gold bearing property of pyrite in Jiaodong gold deposit. It is considered that the formation of the Au-As-rich edge of pyrite is controlled by the variation of As content in fluid, while the enrichment of invisible gold in the edge of As bearing pyrite is more likely to be a passive response process. This indicates that there is abnormal addition of As-Au rich fluids in the ore-forming process, which provides clues on the study of "invisible gold" mineralization and the formation of high-grade gold ore in the future. The Jiaodong gold deposit is mainly characterized by visible gold (gold particle) mineralization. The composition and fineness of gold particles can directly invert the gold mineralization process. The implementation of the series of ultra-deep boreholes in Northwest Jiaodong provides an opportunity to compare the variation mechanism of gold fineness at different depths, and to reveal the temporal and spatial evolution of gold mineralization. Based on the composition and variation of trace elements in pyrite at different depths and the fineness of granular gold, this paper discussed the contribution of deep and shallow water/rock reaction (wall rock sulfidation) and

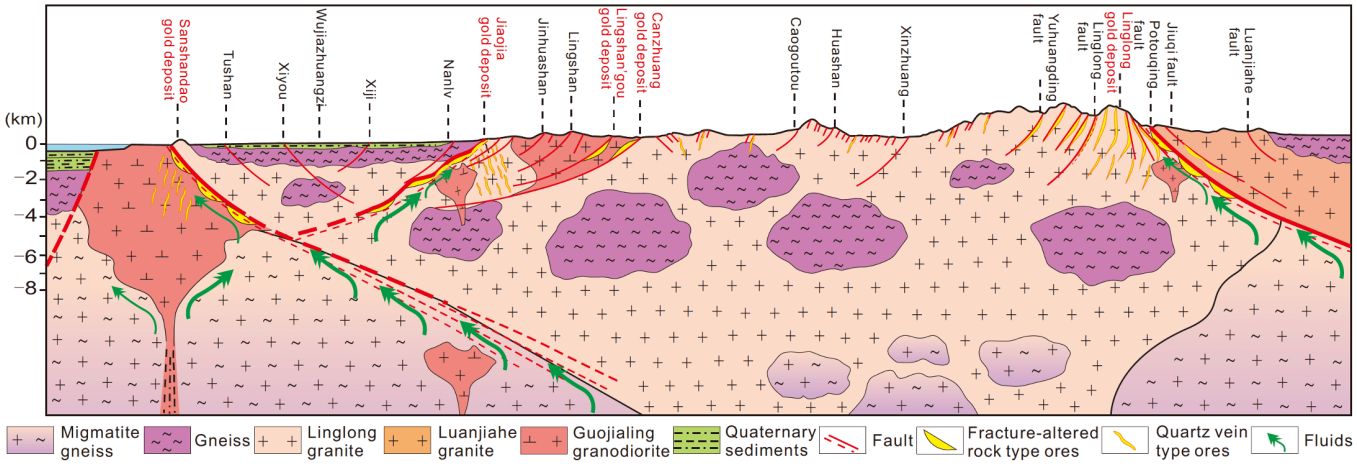

Figure 10 A schematic model for the genesis of the Jiaodong gold deposits.

fluid phase separation to the gold precipitation and mineralization in the Sanshandao gold deposit, which is important for understanding the geochemical barrier causing large-scale metal precipitation and revealing the detailed process of gold mineralization. There are remarkable differences in geological and metallogenic characteristics between the Jiaodong gold deposit and the greenstone belt type gold deposit in the stable craton of the world. To a certain extent, the Jiaodong gold deposit is also different from the orogenic gold deposit proposed in other studies. The destruction of the NCC in the Late Mesozoic is genetically related to the large-scale mineralization in Jiaodong. On the basis of the geological evidence reflected by the discussion of the terminal effect of mineralization, this paper puts forward a genetic model of Jiaodong gold deposit, which is similar to the orogenic gold deposit formed by high-grade metamorphism. It is of great significance to improve the genetic model of craton destruction type gold deposit.

Acknowledgements *We thank two anonymous reviewers, executive Editor-in-Chief academician Yongfei ZHENG, and Responsible Editor Professor Jianwei LI for their insightful comments and detailed reviews, which improved the quality of this manuscript. This work was supported by the National Key Research and Development Program (Grant No. 2016YFC0600105) and the National Natural Science Foundation of China (Grant Nos. 41672094, 41772080).*

References

Anderko A, Pitzer K S. 1993. Equation-of-state representation of phase equilibria and volumetric properties of the system NaCl-H_2O above 573 K. Geochim Cosmochim Acta, 57: 1657–1680

Bodnar R J, Sanchez P L, Moncada D, Steele-MacInnes M. 2014. Fluid inclusions in hydrothermal ore deposits. In: Holland H D, Turekian K K, eds. Treatise Geochem, 13: 119–142

Brooks H L, Steele-MacInnis M. 2019. A model for the solubility of minerals in saline aqueous fluids in the crust and upper mantle. Am J Sci, 319: 754–787

Cai Y C, Fan H R, Santosh M, Liu X, Hu F F, Yang K F, Lan T G, Yang Y H, Liu Y. 2013. Evolution of the lithospheric mantle beneath the southeastern North China Craton: Constraints from mafic dikes in the Jiaobei terrain. Gondwana Res, 24: 601–621

Cameron E M. 1989. Scouring of gold from the lower crust. Geology, 17: 26–29

Cook N J, Ciobanu C L, Meria D, Silcock D, Wade B. 2013. Arsenopyrite-pyrite association in an orogenic gold ore: Tracing mineralization history from textures and trace elements. Econ Geol, 108: 1273–1283

Davidson J, Turner S, Handley H, MacPherson C, Dosseto A. 2007. Amphibole "sponge" in arc crust? Geology, 35: 787–790

Deng J, Qiu K F, Wang Q F, Goldfarb R, Yang L Q, Zi J W, Geng J Z, Ma Y. 2020. *In-situ* dating of hydrothermal monazite and implications on the geodynamic controls of ore formation in the Jiaodong gold province, eastern China. Econ Geol, 115: 671–685

Deng J, Wang C, Bagas L, Carranza E J M, Lu Y. 2015. Cretaceous-Cenozoic tectonic history of the Jiaojia Fault and gold mineralization in the Jiaodong Peninsula, China: Constraints from zircon U-Pb, illite K-Ar, and apatite fission track thermochronometry. Miner Depos, 50: 987–1006

Diamond L W. 2001. Review of the systematics of CO_2-H_2O fluid inclusions. Lithos, 55: 69–99

Driesner T, Heinrich C A. 2007. The system H_2O-NaCl. Part I: Correlation formulae for phase relations in temperature-pressure-composition space from 0 to 1000℃, 0 to 5000 bar, and 0 to 1 XNaCl. Geochim Cosmochim Acta, 71: 4880–4901

Duan Z, Møller N, Weare J H. 1995. Equation of state for the NaCl-H_2O-CO_2 system: Prediction of phase equilibria and volumetric properties. Geochim Cosmochim Acta, 59: 2869–2882

Elmer F L, White R W, Powell R. 2006. Devolatilization of metabasic rocks during greenschist-amphibolite facies metamorphism. J Metamorph Geol, 24: 497–513

Fan H R, Feng K, Li X H, Hu F F, Yang KF. 2016. Mesozoic gold mineralization in the Jiaodong and Korean Peninsulas (in Chinese with English abstract). Acta Petrol Sin, 32: 3225–3238

Fan H R, Li X H, Zuo Y B, Chen L, Liu S, Hu F F, Feng K. 2018. *In-situ* LA-(MC)-ICPMS and (Nano)SIMS trace elements and sulfur isotope analyses on sulfides and application to confine metallogenic process of ore deposit (in Chinese with English abstract). Acta Petrol Sin, 34: 3479–3496

Fan H R, Zhai M G, Xie Y H, Yang J H. 2003. Ore-forming fluids associated with granite-hosted gold mineralization at the Sanshandao deposit, Jiaodong gold province, China. Miner Depos, 38: 739–750

Feng K, Fan H R, Groves D I, Yang K F, Hu F F, Liu X, Cai Y C. 2020. Geochronological and sulfur isotopic evidence for the genesis of the post-magmatic, deeply sourced, and anomalously gold-rich Daliuhang orogenic deposit, Jiaodong, China. Miner Depos, 55: 293–308

Feng K, Fan H R, Hu F F, Yang K F, Liu X, Shangguan Y N, Cai Y C, Jiang P. 2018. Involvement of anomalously As-Au-rich fluids in the mineralization of the Heilan'gou gold deposit, Jiaodong, China: Evidence from trace element mapping and *in-situ* sulfur isotope composition. J Asian Earth Sci, 160: 304–321

Fisher N H. 1945. The fineness of gold, with special reference to the Morobe gold field, New Guinea. Econ Geol, 40: 449–495

Fu B, Touret J L R. 2014. From granulite fluids to quartz-carbonate megashear zones: The gold rush. Geosci Front, 5: 747–758

Gammons C H, Williams-Jones A E. 1995. Hydrothermal geochemistry of electrum: Thermodynamic constraints. Econ Geol, 90: 420–432

Goldfarb R J, Santosh M. 2014. The dilemma of the Jiaodong gold deposits: Are they unique? Geosci Front, 5: 139–153

Gottschalk M. 2007. Equations of state for complex fluids. Rev Mineral Geochem, 65: 49–97

Groves D I. 1993. The crustal continuum model for late-Archaean lode-gold deposits of the Yilgarn Block, Western Australia. Mineral Depos, 28: 366–374

Groves D I, Goldfarb R J, Robert F, Hart C J R. 2003. Gold deposits in metamorphic belts: Overview of current understanding, outstanding problems, future research, and exploration significance. Econ Geol, 98: 1–29

Groves D I, Santosh M, Deng J, Wang Q, Yang L, Zhang L. 2020. A holistic model for the origin of orogenic gold deposits and its implications for exploration. Miner Depos, 55: 275–292

Herrington R J, Wilkinson J J. 1993. Colloidal gold and silica in mesothermal vein systems. Geology, 21: 539–542

Hou Z, Zhou Y, Wang R, Zheng Y, He W, Zhao M, Evans N J, Weinberg R F. 2017. Recycling of metal-fertilized lower continental crust: Origin of non-arc Au-rich porphyry deposits at cratonic edges. Geology, 45: 563–566

Hough R M, Butt C R M, Fischer-Buhner J. 2009. The crystallography, metallography and composition of gold. Elements, 5: 297–302

Hu F F, Fan H R, Jiang X H, Li X C, Yang K F, Mernagh T. 2013. Fluid inclusions at different depths in the Sanshandao gold deposit, Jiaodong Peninsula, China. Geofluids, 13: 528–541

Hu F F, Fan H R, Zhai M G, Jin C W. 2006. Fluid evolution in the Rushan lode gold deposit of Jiaodong Peninsula, eastern China. J Geochem Explor, 89: 161–164

Hu H L, Fan H R. 2018. The effect of water/rock interaction for the gold fineness of Jiaojia gold deposit (in Chinese with English abstract). Gold Sci Technol, 26: 559–569

Hu H L, Fan H R, Liu X, Cai Y C, Yang K F, Ma W D. 2020a. Two-stage

gold deposition in response to H_2S loss from a single fluid in the Sizhuang deposit (Jiaodong, China). Ore Geol Rev, 120: 103450
Hu H L, Fan H R, Santosh M, Liu X, Cai Y C, Yang K F. 2020b. Ore-forming processes in the Wang'ershan gold deposit (Jiaodong, China): Insight from microtexture, mineral chemistry and sulfur isotope compositions. Ore Geol Rev, 123: 103600
Huang X L, Xu Y G, Liu D Y. 2004. Geochronology, petrology and geochemistry of the granulite xenoliths from Nushan, east China. Geochim Cosmochim Acta, 68: 127–149
Kusebauch C, Gleeson S A, Oelze M. 2019. Coupled partitioning of Au and As into pyrite controls formation of giant Au deposits. Sci Adv, 5: eaav5891
Large R R, Bull S W, Maslennikov V V. 2011. A carbonaceous sedimentary source-rock model for Carlin-type and orogenic gold deposits. Econ Geol, 106: 331–358
Large R R, Danyushevsky L, Hollit C, Maslennikov V, Meffre S, Gilbert S, Bull S, Scott R, Emsbo P, Thomas H, Singh B, Foster J. 2009. Gold and trace element zonation in Pyrite using a laser imaging technique: Implications for the timing of gold in orogenic and Carlin-Style sediment-hosted deposits. Econ Geol, 104: 635–668
Li D, Duan Z. 2007. The speciation equilibrium coupling with phase equilibrium in the H_2O-CO_2-NaCl system from 0 to 250℃, from 0 to 1000 bar, and from 0 to 5 molality of NaCl. Chem Geol, 244: 730–751
Li J W, Vasconcelos P, Zhou M F, Zhao X F, Ma C Q. 2006. Geochronology of the Pengjiakuang and Rushan gold deposits, eastern Jiaodong gold province, northeastern China: Implications for regional mineralization and geodynamic setting. Econ Geol, 101: 1023–1038
Li L, Santosh M, Li S R. 2015. The 'Jiaodong type' gold deposits: Characteristics, origin and prospecting. Ore Geol Rev, 65: 589–611
Li S R, Santosh M. 2014. Metallogeny and craton destruction: Records from the North China Craton. Ore Geol Rev, 56: 376–414
Li X C, Fan H R, Santosh M, Hu F F, Yang K F, Lan T G. 2013. Hydrothermal alteration associated with Mesozoic granite-hosted gold mineralization at the Sanshandao deposit, Jiaodong gold province, China. Ore Geol Rev, 53: 403–421
Li X H, Fan H R, Zhang Y W, Hu F F, Yang K F, Liu X, Cai Y C, Zhao K D. 2018a. Rapid exhumation of the northern Jiaobei Terrane, North China Craton in the Early Cretaceous: Insights from Al-in-hornblende barometry and U-Pb geochronology. J Asian Earth Sci, 160: 365–379
Li X H, Fan H R, Yang K F, Hollings P, Liu X, Hu F F, Cai Y C. 2018b. Pyrite textures and compositions from the Zhuangzi Au deposit, southeastern North China Craton: Implication for ore-forming processes. Contrib Mineral Petrol, 173: 73
Li X H, Klyukin Y I, Steele-MacInnis M, Fan H R, Yang K F, Zoheir B. 2020. Phase equilibria, thermodynamic properties, and solubility of quartz in saline-aqueous-carbonic fluids: Application to orogenic and intrusion-related gold deposits. Geochim Cosmochim Acta, 283: 201–221
Liu Y S, Gao S, Jin S Y, Hu S H, Sun M, Zhao Z B, Feng J L. 2001. Geochemistry of lower crustal xenoliths from Neogene Hannuoba basalt, North China craton: Implications for petrogenesis and lower crustal composition. Geochim Cosmochim Acta, 65: 2589–2604
Ma W D, Fan H R, Liu X, Pirajno F, Hu F F, Yang K F, Yang Y H, Xu W G, Jiang P. 2017. Geochronological framework of the Xiadian gold deposit in the Jiaodong province, China: Implications for the timing of gold mineralization. Ore Geol Rev, 86: 196–211
Ma W D, Fan H R, Liu X, Yang K F, Hu F F, Zhao K, Cai Y C, Hu H L. 2018. Hydrothermal fluid evolution of the Jintingling gold deposit in the Jiaodong peninsula, China: Constraints from U-Pb age, CL imaging, fluid inclusion and stable isotope. J Asian Earth Sci, 160: 287–303
Manning C E. 2018. Fluids of the lower crust: Deep is different. Annu Rev Earth Planet Sci, 46: 67–97
Mao S, Hu J, Zhang Y, Lü M. 2015. A predictive model for the PVTx properties of CO_2-H_2O-NaCl fluid mixture up to high temperature and high pressure. Appl Geochem, 54: 54–64
Meng F C, Sun D S, Cun G. 1998. The fineness of native gold and its indicative significance in Jiaodong gold mines. Gold Geology, 4: 30–32
Miao L, Luo Z, Huang J, Guan K, Wang G L, Mcnaughton J N, Groves I D. 1997. Zircon sensitive high resolution ion microprobe (SHRIMP) study of granitoid intrusions in the Zhaoye gold belt of Shandong province and its implication. Sci China Ser D-Earth Sci, 40: 361–369
Mikhlin Y, Romanchenko A, Likhatski M, Karacharov A, Erenburg S, Trubina S. 2011. Understanding the initial stages of precious metals precipitation: Nanoscale metallic and sulfidic species of gold and silver on pyrite surfaces. Ore Geol Rev, 42: 47–54
Mills S E, Tomkins A G, Weinberg R F, Fan H R. 2015a. Anomalously silver-rich vein-hosted mineralisation in disseminated-style gold deposits, Jiaodong gold district, China. Ore Geol Rev, 68: 127–141
Mills S E, Tomkins A G, Weinberg R F, Fan H R. 2015b. Implications of pyrite geochemistry for gold mineralisation and remobilisation in the Jiaodong gold district, northeast China. Ore Geol Rev, 71: 150–168
Moncada D, Rimstidt J D, Bodnar R J. 2019. How to form a giant epithermal precious metal deposit: Relationships between fluid flow rate, metal concentration of ore-forming fluids, duration of the ore-forming process, and ore grade and tonnage. Ore Geol Rev, 113: 103066
Morrison G W, Rose W J, Jaireth S. 1991. Geological and geochemical controls on the silver content (fineness) of gold in gold-silver deposits. Ore Geol Rev, 6: 333–364
Naden J, Shepherd T J. 1989. Role of methane and carbon dioxide in gold deposition. Nature, 342: 793–795
Palenik C S, Utsunomiya S, Reich M, Kesler S E, Wang L, Ewing R C. 2004. "Invisible" gold revealed: Direct imaging of gold nanoparticles in a Carlin-type deposit. Am Miner, 89: 1359–1366
Pal'yanova G. 2008. Physicochemical modeling of the coupled behavior of gold and silver in hydrothermal processes: Gold fineness, Au/Ag ratios and their possible implications. Chem Geol, 255: 399–413
Patten C G C, Pitcairn I K, Molnár F, Kolb J, Beaudoin G, Guilmette C, Peillod A. 2020. Gold mobilization during metamorphic devolatilization of Archean and Paleoproterozoic metavolcanic rocks. Geology, 48: 1110–1114
Peng H W, Fan H R, Liu X, Wen B J, Zhang Y W, Feng K. 2021. New insights into the control of visible gold fineness and deposition: A case study of the Sanshandao gold deposit (Jiaodong, China).. Am Miner, 106: 135–149
Peterson E C, Mavrogenes J A. 2014. Linking high-grade gold mineralization to earthquake-induced fault-valve processes in the Porgera gold deposit, Papua New Guinea. Geology, 42: 383–386
Phillips G N, Powell R. 2009. Formation of gold deposits: Review and evaluation of the continuum model. Earth-Sci Rev, 94: 1–21
Phillips G N, Powell R. 2010. Formation of gold deposits: A metamorphic devolatilization model. J Metamorph Geol, 28: 689–718
Ping X, Zheng J, Xiong Q, Griffin W L, Yu C, Su Y. 2019. Downward rejuvenation of the continental lower crust beneath the southeastern North China Craton. Tectonophysics, 750: 213–228
Pokrovski G S, Akinfiev N N, Borisova A Y, Zotov A V, Kouzmanov K. 2014. Gold speciation and transport in geological fluids: Insights from experiments and physical-chemical modelling. Geol Soc Lond Spec Publ, 402: 9–70
Pokrovski G S, Dubrovinsky L S. 2011. The S3− ion is stable in geological fluids at elevated temperatures and pressures. Science, 331: 1052–1054
Qiu Y, Groves D I, McNaughton N J, Wang L, Zhou T. 2002. Nature, age, and tectonic setting of granitoid-hosted, orogenic gold deposits of the Jiaodong Peninsula, eastern North China craton, China. Miner Depos, 37: 283–305
Reed M H, Palandri J. 2006. Sulfide mineral precipitation from hydrothermal fluids. Rev Mineral Geochem, 61: 609–631
Reich M, Deditius A, Chryssoulis S, Li J W, Ma C Q, Parada M A, Barra F, Mittermayr F. 2013. Pyrite as a record of hydrothermal fluid evolution in a porphyry copper system: A SIMS/EMPA trace element study. Geochim Cosmochim Acta, 104: 42–62
Reich M, Kesler S E, Utsunomiya S, Palenik C S, Chryssoulis S L, Ewing R C. 2005. Solubility of gold in arsenian pyrite. Geochim Cosmochim

Acta, 69: 2781 –2796
Ridley J R, Diamond L W. 2000. Fluid chemistry of orogenic lode gold deposits and implications for genetic models. Society of Economic Geologists, Rev Econ Geol, 13: 141–162
Román N, Reich M, Leisen M, Morata D, Barra F, Deditius A P. 2019. Geochemical and micro-textural fingerprints of boiling in pyrite. Geochim Cosmochim Acta, 246: 60–85
Saunders J, Burke M. 2017. Formation and aggregation of gold (electrum) nanoparticles in epithermal ores. Minerals, 7: 163
Song M C, Song Y X, Ding Z J, Wei X F, Sun S L, Song G Z, Zhang J J, Zhang P J, Wang Y G. 2019. The discovery of the Jiaojia and the Sanshandao giant gold deposits in Jiaodong peninsula and discussion on the relevant issues (in Chinese with English abstract). Geotect Metal, 43: 92–110
Starr P G, Pattison D R M. 2019. Metamorphic devolatilization of basalts across the greenschist-amphibolite facies transition zone: Insights from isograd mapping, petrography and thermodynamic modelling. Lithos, 342-343: 295–314
Steele-MacInnis M. 2018. Fluid inclusions in the system H_2O-NaCl-CO_2: An algorithm to determine composition, density and isochore. Chem Geol, 498: 31–44
Stefánsson A, Seward T M. 2004. Gold(I) complexing in aqueous sulphide solutions to 500°C at 500 bar. Geochim Cosmochim Acta, 68: 4121–4143
Su W, Zhang H, Hu R, Ge X, Xia B, Chen Y, Zhu C. 2012. Mineralogy and geochemistry of gold-bearing arsenian pyrite from the Shuiyindong Carlin-type gold deposit, Guizhou, China: Implications for gold depositional processes. Miner Depos, 47: 653–662
Sun W, Ding X, Hu Y H, Li X H. 2007. The golden transformation of the Cretaceous plate subduction in the west Pacific. Earth Planet Sci Lett, 262: 533–542
Sun Y X, Yu X F, Dan W, Xiong Y X, Zhang Y, Chi N J, Shu L, Li M, Chen W. 2020. Mineralization characteristics and modes of occurrence of gold minerals at the depth of 3000 meters in Jiaojia fault zone, Jiaodong Peninsula (in Chinese with English abstract). Acta Geosci Sin, 41: 919–937
Tan J, Wei J, He H, Su F, Li Y, Fu L, Zhao S, Xiao G, Zhang F, Xu J, Liu Y, Stuart F M, Zhu R. 2018. Noble gases in pyrites from the Guocheng-Liaoshang gold belt in the Jiaodong province: Evidence for a mantle source of gold. Chem Geol, 480: 105–115
Tang H, Zheng J, Griffin W L, O'Reilly S Y, Yu C, Pearson N J, Ping X, Xia B, Yang H. 2014. Complex evolution of the lower crust beneath the southeastern North China Craton: The Junan xenoliths and xenocrysts. Lithos, 206-207: 113–126
Tomkins A G, Grundy C. 2009. Upper temperature limits of orogenic gold deposit formation: Constraints from the granulite-hosted Griffin's find deposit, Yilgarn Craton. Econ Geol, 104: 669–685
Touret J L R. 2009. Mantle to lower-crust fluid/melt transfer through granulite metamorphism. Rus Geol Geophys, 50: 1052–1062
Trigub A L, Tagirov B R, Kvashnina K O, Lafuerza S, Filimonova O N, Nickolsky M S. 2017. Experimental determination of gold speciation in sulfide-rich hydrothermal fluids under a wide range of redox conditions. Chem Geol, 471: 52–64
Wang Y W, Zhu F S, Gong R T. 2002. Tectonic isotope geochemistry-Further study on sulphur isotope of Jiaodong gold concentration area (in Chinese with English abstract). Gold, 23: 1–16
Wang Z L, Yang L Q, Guo L N, Marsh E, Wang J P, Liu Y, Zhang C, Li R H, Zhang L, Zheng X L, Zhao R X. 2015. Fluid immiscibility and gold deposition in the Xincheng deposit, Jiaodong Peninsula, China: A fluid inclusion study. Ore Geol Rev, 65: 701–717
Wang Z, Cheng H, Zong K, Geng X, Liu Y, Yang J, Wu F, Becker H, Foley S, Wang C Y. 2019. Metasomatized lithospheric mantle for Mesozoic giant gold deposits in the North China craton. Geology, 48: 169–173
Wei Q, Fan H R, Lan T G, Liu X, Jiang X H, Wen BJ. 2015. Genesis of Sizhuang gold deposit, Jiaodong Peninsula: Evidences from fluid inclusion and quartz solubility modeling (in Chinese with English abstract). Acta Petrol Sin, 31: 1049–1062
Wen B J, Fan H R, Santosh M, Hu F F, Pirajno F, Yang K F. 2015. Genesis of two different types of gold mineralization in the Linglong gold field, China: Constrains from geology, fluid inclusions and stable isotope. Ore Geol Rev, 65: 643–658
Wen B J, Fan H R, Hu F F, Liu X, Yang K F, Sun Z F, Sun Z F. 2016. Fluid evolution and ore genesis of the giant Sanshandao gold deposit, Jiaodong gold province, China: Constrains from geology, fluid inclusions and H–O–S–He–Ar isotopic compositions. J Geochem Explor, 171: 96–112
Williams-Jones A E, Heinrich C A. 2005. Vapor transport of metals and the formation of magmatic-hydrothermal ore deposits. Econ Geol, 100: 1287–1312
Wu Y F, Evans K, Li J W, Fougerouse D, Large R R, Guagliardo P. 2019a. Metal remobilization and ore-fluid perturbation during episodic replacement of auriferous pyrite from an epizonal orogenic gold deposit. Geochim Cosmochim Acta, 245: 98–117
Wu F Y, Yang J H, Xu Y G, Wilde S A, Walker R J. 2019b. Destruction of the North China Craton in the Mesozoic. Annu Rev Earth Planet Sci, 47: 173–195
Xia Q K, Liu J, Kovács I, Hao Y T, Li P, Yang X Z, Chen H, Sheng Y M. 2017. Water in the upper mantle and deep crust of eastern China: Concentration, distribution and implications. Natl Sci Rev, 6: 125–144
Xing Y, Brugger J, Tomkins A, Shvarov Y. 2019. Arsenic evolution as a tool for understanding formation of pyritic gold ores. Geology, 47: 335–338
Xiong L, Zhao X, Wei J, Jin X, Fu L, Lin Z. 2020. Linking Mesozoic lode gold deposits to metal-fertilized lower continental crust in the North China Craton: Evidence from Pb isotope systematics. Chem Geol, 533: 119440
Xu W G, Fan H R, Yang K F, Hu F F, Cai Y C, Wen B J. 2016. Exhaustive gold mineralizing processes of the Sanshandao gold deposit, Jiaodong Peninsula, eastern China: Displayed by hydrothermal alteration modeling. J Asian Earth Sci, 129: 152–169
Yang J H, Zhou X H. 2001. Rb-Sr, Sm-Nd, and Pb isotope systematics of pyrite: Implications for the age and genesis of lode gold deposits. Geology, 29: 711–714
Yang K F, Fan H R, Santosh M, Hu F F, Wilde S A, Lan T G, Lu L N, Liu Y S. 2012. Reactivation of the Archean lower crust: Implications for zircon geochronology, elemental and Sr-Nd-Hf isotopic geochemistry of late Mesozoic granitoids from northwestern Jiaodong Terrane, the North China Craton. Lithos, 146-147: 112–127
Yang K F, Jiang P, Fan H R, Zuo Y B, Yang Y H. 2018. Tectonic transition from a compressional to extensional metallogenic environment at ~120 Ma revealed in the Hushan gold deposit, Jiaodong, North China Craton. J Asian Earth Sci, 160: 408–425
Yang L Q, Deng J, Wang Z L, Guo L N, Li R H, Groves D I, Danyushevsky L V, Zhang C, Zheng X L, Zhao H. 2016. Relationships between gold and pyrite at the Xincheng gold deposit, Jiaodong Peninsula, China: Implications for gold source and deposition in a brittle epizonal environment. Econ Geol, 111: 105–126
Ying J F, Zhang H F, Tang Y J. 2010. Lower crustal xenoliths from Junan, Shandong province and their bearing on the nature of the lower crust beneath the North China Craton. Lithos, 119: 363–376
Yu G, Xu T, Ai Y, Chen L, Yang J. 2020. Significance of crustal extension and magmatism to gold deposits beneath Jiaodong Peninsula, eastern North China Craton: Seismic evidence from receiver function imaging with a dense array. Tectonophysics, 789: 228532
Yuan Z Z, Li Z K, Zhao X F, Sun H S, Qiu H N, Li J W. 2019. New constraints on the genesis of the giant Dayingezhuang gold (silver) deposit in the Jiaodong district, North China Craton. Ore Geol Rev, 112: 103038
Zhang H F. 2012. Destruction of ancient lower crust through magma underplating beneath Jiaodong Peninsula, North China Craton: U-Pb and Hf isotopic evidence from granulite xenoliths. Gondwana Res, 21: 281–292
Zhang L, Weinberg R F, Yang L Q, Groves D I, Sai S X, Matchan E, Phillips D, Kohn B P, Miggins D P, Liu Y, Deng J. 2020. Mesozoic

orogenic gold mineralization in the Jiaodong Peninsula, China: A focused event at 120±2 Ma during cooling of pregold granite intrusions. Econ Geol, 115: 415–441
Zhang Y W, Hu F F, Fan H R, Liu X, Feng K, Cai Y C. 2020. Fluid evolution and gold precipitation in the Muping gold deposit (Jiaodong, China): Insights from *in-situ* trace elements and sulfur isotope of sulfides. J Geochem Explor, 218: 106617
Zheng J P, Griffin W L, Ma Q, O'Reilly S Y, Xiong Q, Tang H Y, Zhao J H, Yu C M, Su Y P. 2012. Accretion and reworking beneath the North China Craton. Lithos, 149: 61–78
Zheng Y, Mao J, Chen Y, Sun W, Ni P, Yang X. 2019. Hydrothermal ore deposits in collisional orogens. Sci Bull, 64: 205–212
Zheng Y F, Xiao W J, Zhao G. 2013. Introduction to tectonics of China. Gondwana Res, 23: 1189–1206
Zheng Y, Xu Z, Zhao Z, Dai L. 2018. Mesozoic mafic magmatism in North China: Implications for thinning and destruction of cratonic lithosphere. Sci China Earth Sci, 61: 353–385
Zhong R, Brugger J, Tomkins A G, Chen Y, Li W. 2015. Fate of gold and base metals during metamorphic devolatilization of a pelite. Geochim Cosmochim Acta, 171: 338–352
Zhu R X, Fan H R, Li J W, Meng Q R, Li S R, Zeng Q D. 2015. Decratonic gold deposits. Sci China Earth Sci, 58: 1523–1537

(Responsible editor: Jianwei LI)